ELSEVIER

Journal of Fluids and Structures 24 (2008) 883–906

JOURNAL OF FLUIDS AND STRUCTURES

www.elsevier.com/locate/jfs

Numerical simulation of flow around an orbiting cylinder at different ellipticity values

L. Baranyi*

Department of Fluid and Heat Engineering, University of Miskolc, H-3515 Miskolc-Egyetemváros, Hungary

Received 29 November 2006; accepted 7 December 2007
Available online 4 March 2008

Abstract

This paper deals with the numerical simulation of low Reynolds number flow (Re = 120–180) past a circular cylinder in orbital motion. The Navier–Stokes equations, pressure Poisson equations and continuity are written in primitive variables in a noninertial system fixed to the orbiting cylinder and solved by the finite difference method. Ellipticity values between 0 and 1.2 (from pure in-line oscillation through a full circle and beyond) were investigated. Sudden changes in state (jumps) are found when time-mean or root-mean-square values of force coefficients or energy transfer are plotted against ellipticity. Pre- and post-jump analysis was carried out by investigating limit cycles, time-histories, phase angles and flow patterns. These investigations revealed that ellipticity can have a large effect on the energy transfer between the incompressible fluid and a circular cylinder forced to follow an orbital path, and that small changes in the amplitude of transverse motion can have a dramatic effect. The phase angle was altered by about 180° at the jumps. Also investigated were the direction of orbit, which affects the state curves belonging to the time-mean values of lift only, and the effect of initial conditions, which alters the location of jumps without changing the state curves.

Keywords: Energy transfer; Limit cycle curves; Low Reynolds number; Navier–Stokes; Orbiting cylinder; Phase angle

1. Introduction

The near-wake structure of bluff bodies is extremely complex, and it seems that a theoretical approach cannot fully clarify this structure. For this purpose, either experimental or numerical analysis is needed. A literature survey reveals that many investigations have been performed of near-wake flow structure subject to controlled forcing, where the body is mechanically moved. In general, relatively simple forcing methods on the cylinder have been employed, e.g., in-line or transverse oscillation, rotational oscillation or orbital oscillation. However, in contrast to the fairly large number of studies conducted on the in-line, transverse and rotational oscillation cases [see for example, transverse oscillation: Öngören and Rockwell (1988), Williamson and Roshko (1988), Anagnostopoulos (1989), Meneghini and Bearman (1995), Lu and Dalton (1996), Kocabiyik and Nguyen (1999), Blackburn and Henderson (1999), Kaiktsis et al. (2004); in-line oscillation: Mureithi et al. (2004), Mureithi and Rodriguez (2005, 2006), Al-Mdallal et al. (2007); rotational oscillation: Tokumaru and Dimotakis (1991), Baek and Sung (2000), Dennis et al. (2000), Poncet (2004), Al-Mdallal and Kocabiyik (2006)], there is relatively little research carried out for the orbital motion.

*Tel.: +36 46 565154; fax: +36 46 565471.
E-mail address: arambl@uni-miskolc.hu

0889-9746/$ - see front matter
doi:10.1016/j.jfluidstructs.2007.12.006

Nomenclature

a_0	cylinder acceleration, nondimensionalised by U^2/d
$A_{x,y}$	amplitude of oscillation in x- or y-directions, respectively, nondimensionalised by d
aclw	anticlockwise (counterclockwise)
clw	clockwise
C_D	drag coefficient, $2F_D/(\rho U^2 d)$
C_{Dv}	viscous drag coefficient (drag due to skin friction)
C_L	lift coefficient, $2F_L/(\rho U^2 d)$
C_{pb}	base pressure coefficient
d	cylinder diameter, length scale (m)
D	dilation, nondimensionalised by U/d
e	ellipticity, A_y/A_x
E	mechanical energy transfer per motion cycle, nondimensionalised by $\rho U^2 d^2/2$
f	oscillation frequency, nondimensionalised by U/d
$\mathbf{F}$	force per unit length of cylinder, $F_D\mathbf{i}+F_L\mathbf{j}$ (N/m)
F_D	drag per unit length of cylinder (N/m)
F_L	lift per unit length of cylinder (N/m)
$\mathbf{i}$, $\mathbf{j}$	unit vectors in x- and y-directions, respectively
$\mathbf{n}$	unit normal vector
p	pressure, nondimensionalised by ρU^2
R	radius, nondimensionalised by d
rms	root-mean-square value
Re	Reynolds number, Ud/v
St	nondimensional vortex shedding frequency, Strouhal number, fd/U
St_0	nondimensional vortex shedding frequency for stationary cylinder at a given Re
t, τ	time, nondimensionalised by d/U
T	motion period, nondimensionalised by d/U
TMV	time-mean value
U	free-stream velocity, velocity scale (m/s)
u, v	velocities in x- and y-directions, nondimensionalised by U
$\mathbf{v}_0$	cylinder velocity, nondimensionalised by U
x, y	Cartesian coordinates, nondimensionalised by d
Δt	time step, nondimensionalised by d/U
Θ	polar angle for initial cylinder position, measured clockwise from positive x-axis
v	kinematic viscosity (m^2/s)
ξ, η	curvilinear coordinates
ρ	fluid density (kg/m^3)
Φ	phase angle

Subscripts

L	lift
D	drag
mean	time-mean value (also denoted by overbar)
rms	root-mean-square value
n	normal
pot	potential flow
x, y	components in x- and y-directions
1,2	for energy transfer in y- and x-directions, respectively; on the cylinder surface and at the outer boundary of the domain, respectively
0	for cylinder motion
ξ, η	curvilinear coordinates

When the cylindrical body performs a combination of in-line and transverse oscillations, such as in tube bundles of heat exchangers, the cylinder follows a closed orbit of an elliptical type. This type of motion can be used, for instance, to model the wave motion around cylindrical bodies. The review paper by Williamson and Govardhan (2004) summarises the recent fundamental results concerning vortex-induced vibrations and discusses the relationship between forced and free vibration results. The ultimate aim in the above-mentioned studies is to investigate the fluid–structure interaction of an elastically supported body or structure placed in a moving flow and, in particular, the mechanical energy transfer between the fluid and the body.

Oscillatory flow has been fairly widely researched [e.g., Bearman et al. (1995), Sarpkaya (1986, 2001), Chaplin and Subbiah (1996)]. Orbital flow, in which the fluid particles follow a closed orbit, has been investigated among others by Chen et al. (1995), who modelled the flow about a stationary horizontal cylinder placed in an orbital flow. As for orbital motion of the cylinder, in fluid at rest an orbiting cylinder has been investigated numerically in Teschauer et al. (2002), following a circular path only, since they were investigating a model of stirring. Williamson et al. (1998), in an experimental study modelling a horizontal cylinder under waves, forced a cylinder to follow an elliptical orbit in still fluid. In a numerical study, using both rough and hybrid meshes, Borthwick (1986) investigated the flow past a rotating cylinder following a circular orbit, placed in a current. Stansby and Rainey (2001) carried out a numerical investigation of the flow around an orbiting cylinder, only in a circular orbit, with a flexibly mounted cylinder in a current. Didier and Borges (2008) performed a numerical analysis of the flow around a mechanically oscillated cylinder in three cases: transverse oscillation, in-line oscillation, or the combination of these two, yielding a fully circular orbital path. In all

three cases, the cylinders were placed in an otherwise uniform flow and the frequency of forced oscillation was varied over a broad range, and three pairs of maximum cylinder velocity components were tested for the oscillating cylinders (one pair was used for the orbital cylinder). They were able to identify the lock-in phenomenon in all three cases. Of the limited number of studies concerning flow around circular cylinders forced to follow an orbital path in an otherwise uniform flow, none address the effect of varying ellipticity values on the force coefficients or energy transfer between cylinder and fluid. Besides being of interest as fundamental research, an elliptically orbiting cylinder in uniform flow can model the flow around a moving cylinder in waves far below the free surface.

Among the studies investigating forced transverse oscillation of a cylinder in uniform flow, Lu and Dalton (1996) and Blackburn and Henderson (1999) have found sudden switches in streamline patterns. In these studies, the amplitude of oscillation was fixed and the frequency of cylinder oscillation was varied in the vicinity of the natural vortex shedding frequency from a fixed cylinder at the same Reynolds number. Both studies found a sudden switch in flow patterns within a very narrow frequency range, as well as a change in the phase angle between the unsteady lift coefficient and the transverse cylinder displacement of about 180°. Blackburn and Henderson (1999) further demonstrated that the switch is associated with a change in the sign of energy transfer between cylinder and fluid. They attributed this switch to the competition between two vorticity production mechanisms, as it did not occur when just one mechanism was present. The present paper describes a similar phenomenon for a more complex flow.

The present study deals with an orbiting cylinder, in forced motion, placed in a uniform flow at low Reynolds numbers. Mechanical energy transfer, phase angle, and time-mean and root-mean-square values of lift, drag, and base pressure coefficients are investigated under lock-in conditions to further investigate sudden switches in vortex structure in the wake of an orbiting cylinder. Ellipticity is varied from 0 (pure in-line oscillation) through a circular orbit (1.0) and beyond, to 1.2. In addition, the effect of orbital direction (clockwise or anticlockwise) and initial condition (the cylinder position at the time when computations are started) are also analysed, unlike the majority of the previous studies on flow past an orbiting cylinder. The objective of the paper is to investigate further the phenomenon of sudden changes in vortex structure while changing the ellipticity of the orbital path.

2. Numerical approach and validation

2.1. Governing equations and boundary conditions

A noninertial system fixed to the cylinder is used to compute two-dimensional (2-D) low-Reynolds number unsteady flow around a circular cylinder placed in a uniform stream and forced to follow an orbital path. The nondimensional Navier–Stokes equations for incompressible constant-property Newtonian fluid, the equation of continuity and the Poisson equation for pressure are as follows:

$$\frac{\partial u}{\partial t}+u\frac{\partial u}{\partial x}+v\frac{\partial u}{\partial y}=-\frac{\partial p}{\partial x}+\frac{1}{\mathrm{Re}}\nabla^2 u-a_{0x}, \tag{1}$$

$$\frac{\partial v}{\partial t}+u\frac{\partial v}{\partial x}+v\frac{\partial v}{\partial y}=-\frac{\partial p}{\partial y}+\frac{1}{\mathrm{Re}}\nabla^2 v-a_{0y}, \tag{2}$$

$$D=\frac{\partial u}{\partial x}+\frac{\partial v}{\partial y}=0, \tag{3}$$

$$\frac{\partial^2 p}{\partial x^2}+\frac{\partial^2 p}{\partial y^2}=2\left[\frac{\partial u}{\partial x}\frac{\partial v}{\partial y}-\frac{\partial u}{\partial y}\frac{\partial v}{\partial x}\right]-\frac{\partial D}{\partial t}. \tag{4}$$

In these equations, u and v are the x and y components of velocity, t is time, p is the pressure, Re is the Reynolds number based on cylinder diameter d, free-stream velocity U, and kinematic viscosity ν, and D is the dilation. Although D is theoretically equal to 0 by continuity, it is kept in Eq. (4) to avoid the accumulation of numerical errors.

The boundary conditions are as follows:

$$(R_1)\quad \text{cylinder surface}: \quad u=v=0, \tag{5}$$

$$\frac{\partial p}{\partial n}=\frac{1}{\mathrm{Re}}\nabla^2 v_n-a_{0n}. \tag{6}$$

$$(R_2) \quad \text{undisturbed domain}: \quad u = u_{\text{pot}} - u_0, v = v_{\text{pot}} - v_0, \tag{7}$$

$$\frac{\partial p}{\partial n} = \left(\frac{\partial p}{\partial n}\right)_{\text{pot}}. \tag{8}$$

On the cylinder surface ($R = R_1 = 0.5$), a no-slip boundary condition is used for the velocity and a Neumann type boundary condition is used for the pressure (see Eqs. (5) and (6)). At the far region ($R = R_2$), potential flow is assumed, as shown by Eqs. (7) and (8). The author is aware of the fact that the potential flow assumption is not valid for the narrow wake domain on (R_2) [see also Baranyi and Shirakashi (1999)]. Our numerical analysis and tests showed, however, that this simplifying assumption results in only a small distortion of the velocity field near the outer boundary wake region. Since our computational results for a stationary cylinder in terms of time-mean and root-mean-square (rms) values of force and base pressure coefficients compared well with experimental and computational values available in the literature, this simplified boundary condition is kept.

2.2. Transformations and numerical approach

To avoid interpolation leading to poor solutions, a boundary-fitted coordinate system is used, allowing boundary conditions to be imposed accurately. By using unique, single-valued functions, the physical domain (x, y, t) can be mapped into a computational domain (ξ, η, τ) as seen in Fig. 1:

$$x(\xi, \eta) = R(\eta)\cos[g(\xi)], \qquad y(\xi, \eta) = -R(\eta)\sin[g(\xi)]; \quad t = \tau, \tag{9}$$

where the dimensionless radius is

$$R(\eta) = R_1 \exp[f(\eta)]. \tag{10}$$

This choice of the structure of the mapping functions automatically assures that the obtained grid is orthogonal on the physical plane for arbitrary functions $g(\xi)$ and $f(\eta)$. In this study, the following linear mapping functions are used:

$$g(\xi) = 2\pi\frac{\xi}{\xi_{\max}}, \qquad f(\eta) = \frac{\eta}{\eta_{\max}}\log\left(\frac{R_2}{R_1}\right), \tag{11}$$

where subscript max refers to maximum value. Using the mapping functions (11), cylindrical coordinates with logarithmically spaced radial cells are obtained on the physical plane, providing a fine grid scale near the cylinder wall and a coarse grid in the far field.

Transformations (9)–(11) are single valued since in this case the Jacobian J

$$J = y_\eta x_\xi - y_\xi x_\eta = \frac{2\pi\log(R_2/R_1)}{\xi_{\max}\eta_{\max}} R^2(\eta) \tag{12}$$

is positive for an arbitrary value of η in the computational domain. In Eq. (12), subscripts ξ and η denote differentiation. Using Eqs. (9)–(11), the governing Eqs. (1)–(4) can also be transformed. The x and y components of the

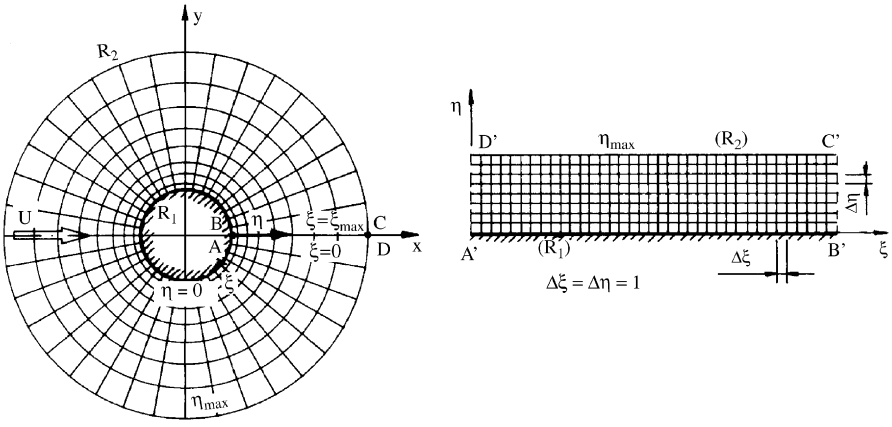

Fig. 1. Mapping of the physical plane.

transformed Navier–Stokes equations are:

$$\frac{\partial u}{\partial \tau}+\frac{1}{J}\left(u\frac{\partial y}{\partial \eta}-v\frac{\partial x}{\partial \eta}\right)\frac{\partial u}{\partial \xi}+\frac{1}{J}\left(v\frac{\partial x}{\partial \xi}-u\frac{\partial y}{\partial \xi}\right)\frac{\partial u}{\partial \eta}=-\frac{1}{J}\left(\frac{\partial y}{\partial \eta}\frac{\partial p}{\partial \xi}-\frac{\partial y}{\partial \xi}\frac{\partial p}{\partial \eta}\right)+\frac{1}{\mathrm{Re}J^2}\left(g_{22}\frac{\partial^2 u}{\partial \xi^2}+g_{11}\frac{\partial^2 u}{\partial \eta^2}\right)-a_{0x}, \tag{13}$$

$$\frac{\partial v}{\partial \tau}+\frac{1}{J}\left(u\frac{\partial y}{\partial \eta}-v\frac{\partial x}{\partial \eta}\right)\frac{\partial v}{\partial \xi}+\frac{1}{J}\left(v\frac{\partial x}{\partial \xi}-u\frac{\partial y}{\partial \xi}\right)\frac{\partial v}{\partial \eta}=-\frac{1}{J}\left(\frac{\partial x}{\partial \xi}\frac{\partial p}{\partial \eta}-\frac{\partial x}{\partial \eta}\frac{\partial p}{\partial \xi}\right)+\frac{1}{\mathrm{Re}J^2}\left(g_{22}\frac{\partial^2 v}{\partial \xi^2}+g_{11}\frac{\partial^2 v}{\partial \eta^2}\right)-a_{0y}. \tag{14}$$

Dilation D transforms as:

$$D=\frac{1}{J}\left(\frac{\partial y}{\partial \eta}\frac{\partial u}{\partial \xi}-\frac{\partial y}{\partial \xi}\frac{\partial u}{\partial \eta}+\frac{\partial x}{\partial \xi}\frac{\partial v}{\partial \eta}-\frac{\partial x}{\partial \eta}\frac{\partial v}{\partial \xi}\right)=0.$$

The Poisson equation for pressure will have the form

$$g_{22}\frac{\partial^2 p}{\partial \xi^2}+g_{11}\frac{\partial^2 p}{\partial \eta^2}=2J\left(\frac{\partial u}{\partial \xi}\frac{\partial v}{\partial \eta}-\frac{\partial u}{\partial \eta}\frac{\partial v}{\partial \xi}\right)-J^2\frac{\partial D}{\partial \tau}. \tag{15}$$

The boundary conditions for pressure, Eqs. (6) and (8), will be transformed as:

$$R=R_1:\frac{\partial p}{\partial \eta}=\frac{g_{11}}{\mathrm{Re}J^2}\left(\frac{\partial x}{\partial \eta}\frac{\partial^2 u}{\partial \eta^2}+\frac{\partial y}{\partial \eta}\frac{\partial^2 v}{\partial \eta^2}\right)-\frac{\partial x}{\partial \eta}a_{0x}-\frac{\partial y}{\partial \eta}a_{0y}, \tag{16}$$

$$R=R_2:\frac{\partial p}{\partial \eta}\cong\frac{R_2}{\eta_{\max}}\log\left(\frac{R_2}{R_1}\right)\left(\frac{\partial p}{\partial n}\right)_{\mathrm{pot}}. \tag{17}$$

In these equations, the elements of the metric tensor will have the form:

$$g_{11}=\left(\frac{\partial x}{\partial \xi}\right)^2+\left(\frac{\partial y}{\partial \xi}\right)^2,\qquad g_{22}=\left(\frac{\partial x}{\partial \eta}\right)^2+\left(\frac{\partial y}{\partial \eta}\right)^2.$$

In Eq. (9), the transformation of domains does not contain time, so the mesh, which is fixed to the cylinder, does not change with time, and therefore the transformed Navier–Stokes Eqs. (13) and (14) do not contain time components for the mesh. The choice of transformations (9)–(11) renders the off-diagonal elements of the metric tensor zero, i.e., $g_{12}=g_{21}=0$, and so the mixed second derivatives are missing from the Laplacian terms in Eqs. (13)–(16). The transformation also ensures that the coefficients of the first-order derivatives in the Laplacian terms in the above equations are zero [e.g., Fletcher (1997)]. Since the mapping is given by elementary functions, the metric parameters and coordinate derivatives can be computed from closed forms, hence numerical differentiation leading to numerical errors can be avoided. The equidistant mesh obtained in the computational plane is beneficial for computational ease.

The grid aspect ratio AR [see Fletcher (1997)], i.e., the ratio of the two sides of an elementary rectangle on the physical plane (see Fig. 1), will have the form:

$$\mathrm{AR}=\sqrt{\frac{g_{22}}{g_{11}}}=\frac{f_\eta}{g_\xi}=\frac{\xi_{\max}\log(R_2/R_1)}{2\pi\eta_{\max}}.$$

It can be seen from this equation that the grid aspect ratio is constant over the whole computational domain. By properly choosing the number of grid points in the ξ and η directions, this constant can be set to unity, resulting in conformal transformation. Since the grid, as well as the noninertial system of this investigation, is fixed to the accelerating cylinder and is generated only once, velocities for grid deformation do not appear in the transformed Navier–Stokes Eqs. (13) and (14). Equations are solved in the 'relative' system fixed to the orbiting cylinder. As the cylinder is in forced motion, the x and y displacements of its origin are prescribed in time, and with this, the velocity and acceleration of the cylinder are also prescribed.

The transformed equations are solved by the finite difference method. Space derivatives are approximated by fourth-order central differences, except for the convective terms for which a third-order modified upwind scheme is used [see Kawamura and Kuwahara (1984)]. The Poisson equation for pressure is solved by the successive over-relaxation (SOR) method, with the residual level of 10^{-5} (this has been found to yield results basically identical to those belonging to the value of 10^{-6}). The Navier–Stokes equations are integrated directly over each time step, so the method is first-order accurate in time. The Poisson equation for pressure contains the time derivative of dilation D, which is theoretically zero for an incompressible fluid. By using this term, the dilation is set to zero at each time step, as suggested by Harlow and Welch (1965), thus satisfying continuity. Very small time steps (0.0005 or 0.00025) are used to compensate for the first-order approach in time. While not optimal computationally, this method gives accurate results.

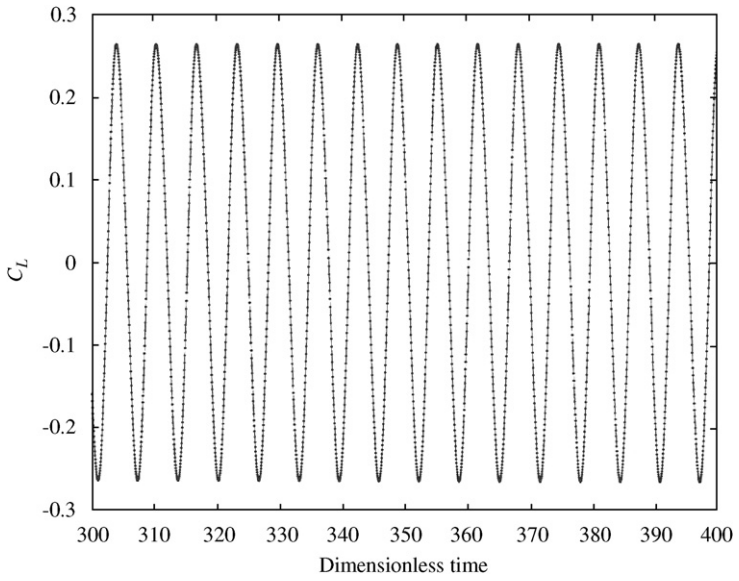

Fig. 2. Time history of fixed body lift coefficient (inertial force removed) for a transversely oscillated cylinder for two combinations of grid and time step (dotted line: 301×177, $\Delta t = 0.0005$; solid line: 481×283, $\Delta t = 0.00025$) ($\mathrm{Re} = 185$, $A_x = 0$, $A_y = 0.2$, $f = 0.8\mathrm{St}_0$, $\mathrm{St}_0 = 0.195$).

The code was worked out for a stationary cylinder and validated, and was extended for an oscillating and then for an orbiting cylinder. Normally, the dimensionless time step was 0.0005 and the number of grid points was 301×177 (the minimal and maximal mesh sizes were $\Delta R_{\min}/d = 0.01059$; $\Delta R_{\max}/d = 0.4148$; the ratio of consecutive mesh sizes was constant at $\Delta r_{i+1}/\Delta r_i = 1.02118$). The effect of grid and time step on the solution was systematically tested by using a second grid of 481×283 ($\Delta R_{\min}/d = 0.00658$; $\Delta R_{\max}/d = 0.2599$; $\Delta r_{i+1}/\Delta r_i = 1.01317 = \text{constant}$) and a time step of 0.00025, which gave very similar results to those of the coarser mesh at the larger time step for both a stationary and a transversely oscillating cylinder. One example is given in Fig. 2, which shows the time-history of lift for a transversely oscillating cylinder ($\mathrm{Re} = 185$, $A_y = 0.2$, $f/\mathrm{St}_0 = 0.8$, $\mathrm{St}_0 = 0.195$) at the two combinations of grid size and time step. Since accuracy was not compromised and computational time is reduced, the majority of computations were carried out using the coarser mesh and larger time step. The computational domain is characterised by $R_2/R_1 = 40$. For each computational case, 80–100 shedding cycles were considered. This was amply sufficient to reach full lock-in (where the frequency of vortex shedding is identical to the frequency of the cylinder oscillation) for an orbiting cylinder for all cases investigated here. To check whether the solution might change over a longer shedding period, 2000 cycles were investigated and the same periodic solution as for 80 cycles was found.

2.3. Code validation for stationary and oscillating cylinders

The 2-D code developed by the author has been extensively tested against experimental and computational results for fixed cylinders and good agreement has been found. In Baranyi and Shirakashi (1999), the comparisons with Strouhal number versus Reynolds number based on Roshko (1954)'s experiments and with the time-mean value (TMV) of drag versus Re chart found in Schlichting (1951). Both results compared well with the experimental results. In Baranyi (2003), the TMV of base pressure coefficients versus Re was compared with the experimental results of Roshko (1993). Again, very good agreement was found except for $\mathrm{Re} = 180$, where probably the presence of 3-D effects makes the measurements inaccurate and unreliable. In Baranyi and Lakatos (2004), the root-mean-square (rms) value of lift coefficient versus Re compared well with experimental results shown in Norberg (2003). Good agreement was obtained for Strouhal number when compared with results obtained by the vortex cloud method, though due to the 'noisy' nature of the vortex cloud method, there was some discrepancy in the rms values of lift and drag obtained by the two methods (Baranyi and Lewis, 2006). A table can be found in the appendix of Baranyi and Lewis (2006) which contains results of the present author for a stationary cylinder: Strouhal number and TMV and rms values of lift, drag, viscous drag, and base pressure coefficients are given for $\mathrm{Re} = 10$–190 in increments of 5, with smaller Re increments around the onset of

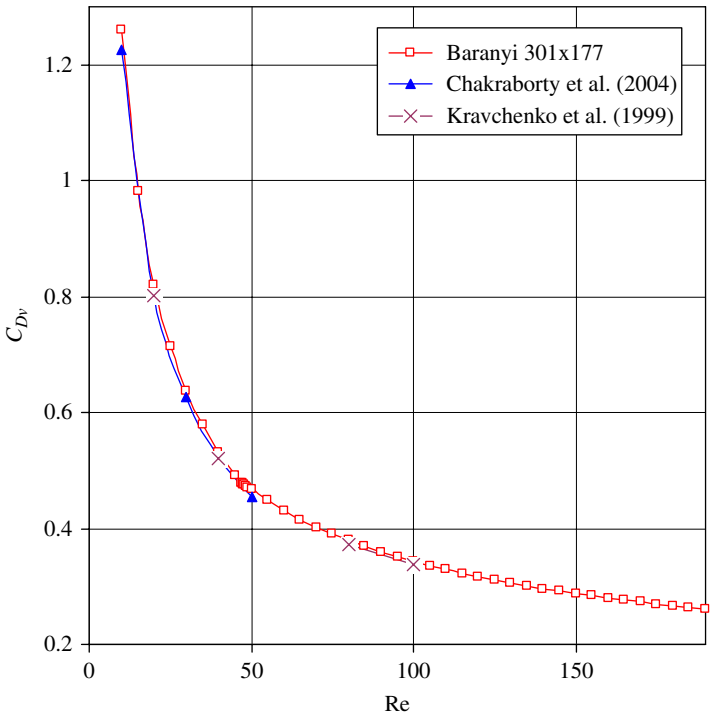

Fig. 3. Results for a stationary cylinder: time-mean viscous drag coefficient $\bar{C}_{Dv}$ versus Reynolds number Re compared with Chakraborty et al. (2004) and Kravchenko et al. (1999).

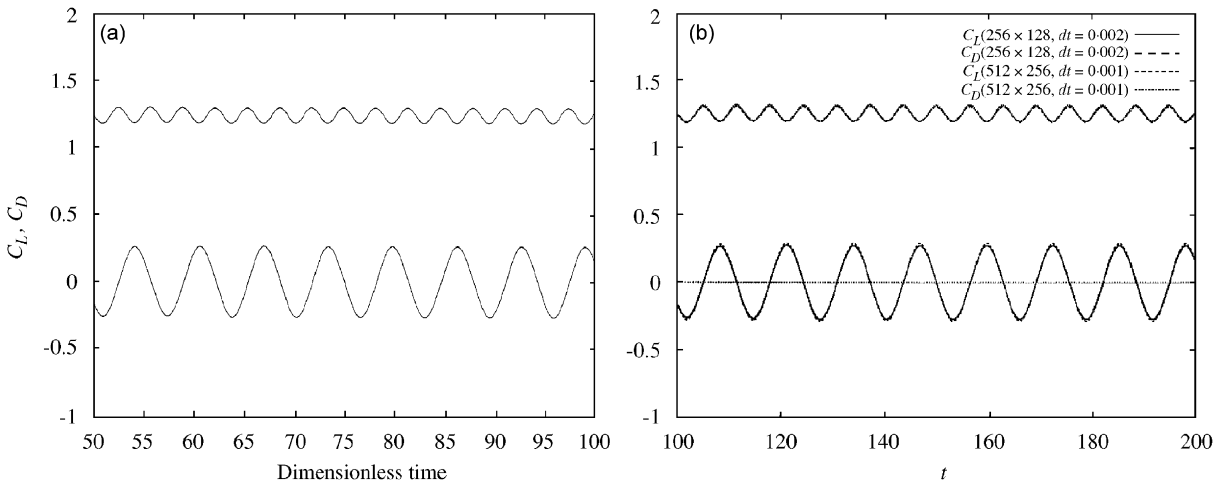

Fig. 4. Time histories (Re = 185, $A_x = 0$, $A_y = 0.2$, $f = 0.8\mathrm{St}_0$, $\mathrm{St}_0 = 0.195$) of fixed body lift and drag coefficients for a transversely oscillated cylinder, comparing (a) Baranyi and (b) Lu and Dalton (1996) (by permission of the publisher).

periodic vortex shedding. A further comparison with computational results for a stationary cylinder can be found in Fig. 3, which shows the TMV of the viscous drag coefficient C_{Dv} versus Reynolds number for the grid size 301×177 and time step 0.0005, and compares them with the results of Chakraborty et al. (2004) for Re = 10–50 and those of Kravchenko et al. (1999) for Re = 20–100. As can be seen, the data compare quite well.

For oscillating cylinders, experimental evidence from Bearman and Obasaju (1982) and Koide et al. (2002) shows that lock-in increases the span-wise correlation of signals and the two-dimensionality of the flow compared to flow around stationary cylinders. Poncet (2004) shows how the 3-D wake behind a circular cylinder can be made 2-D by

using lock-in triggered by rotary oscillation of the cylinder. For this reason, a 2-D code is suitable even at higher Reynolds numbers than the 190 at which three-dimensional effects start to appear for stationary cylinders (Barkley and Henderson, 1996). Lu and Dalton (1996), for instance, used $\mathrm{Re} = 185$, 500 and 1000 in their transverse cylinder oscillation study.

Lu and Dalton (1996), who used a finite difference solution of the unsteady Navier–Stokes equations with a primitive variable formulation, carried out a systematic investigation of flow around a circular cylinder in forced transverse

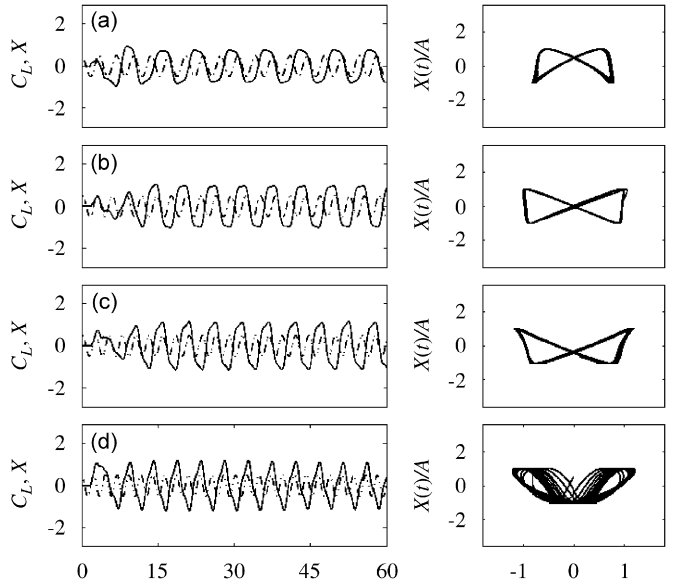

Fig. 5. Time histories of lift coefficient and cylinder displacement (left) and Lissajous patterns of lift coefficient and dimensionless cylinder displacement (right), at frequency ratios of (a) 1.5, (b) 1.75, (c) 1.95, and (d) 2.2, for cylinder oscillating in-line ($\mathrm{Re} = 200$, $A_x = 0.1$, $A_y = 0$, $\mathrm{St}_0 = 0.195$); from Al-Mdallal et al. (2007) (by permission of the publisher).

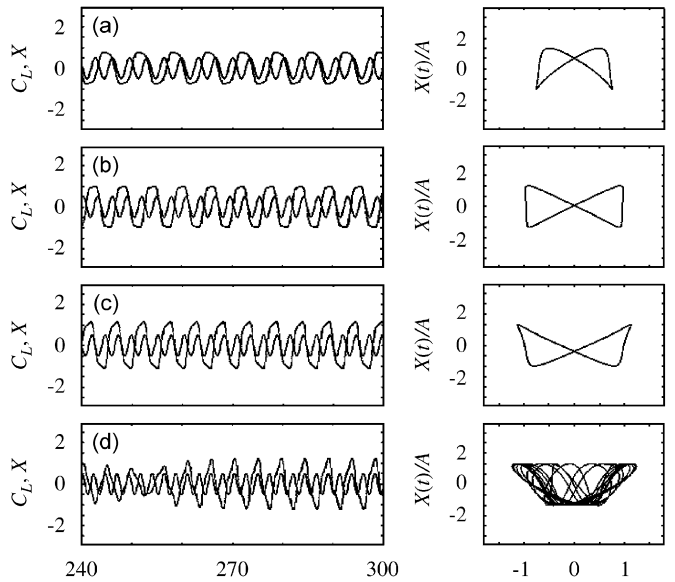

Fig. 6. Time histories of lift coefficient and cylinder displacement (left), Lissajous patterns of lift coefficient and dimensionless cylinder displacement (right), at frequency ratios of (a) 1.5, (b) 1.75, (c) 1.95, and (d) 2.2, for cylinder oscillating in-line ($\mathrm{Re} = 200$, $A_x = 0.1$, $A_y = 0$, $\mathrm{St}_0 = 0.195$).

oscillation at different frequency ratios from 0.8 to 1.2 and at amplitudes 0.4 and 1.0 (or rather 0.2 and 0.5, when the amplitude is nondimensionalised by the cylinder diameter instead of the radius), as well as at Reynolds numbers 185, 500, and 1000. Computations were carried out in order to compare results with those of Lu and Dalton (1996), for the case of $\mathrm{Re} = 185$, $A_y/d = 0.2$, $f/\mathrm{St}_0 = 0.8$ and $\mathrm{St}_0 = 0.195$ at two different grid sizes (for Lu and Dalton, 256×128, $\Delta t = 0.002$; 512×256, $\Delta t = 0.001$ (or, when the time is nondimensionalised by the cylinder diameter rather than the radius, $\Delta t = 0.001$ and 0.0005), and for Baranyi, 301×177, $\Delta t = 0.0005$; 481×283, $\Delta t = 0.00025$). Fig. 4 displays the time-history of lift and drag coefficients from which the inertial forces have been removed (Lu and Dalton term this a 'fixed body' coefficient (see also Baranyi, 2005b), which shows the relationship between force coefficients in inertial and noninertial systems). Fig. 4(a) shows results for 301×177 and $\Delta t = 0.0005$ (see Fig. 2 for results for both grids); results for both of Lu and Dalton's grids are shown in Fig. 4(b) (curves coincide so closely that they cannot be distinguished). The curves from the two studies are very similar to each other, as are the findings for the $C_{D\mathrm{mean}}$ and $C_{L\mathrm{rms}}$: Lu and Dalton report $C_{D\mathrm{mean}} = 1.25$ and $C_{L\mathrm{rms}} = 0.18$ for both grids, Baranyi found $C_{D\mathrm{mean}} = 1.244$ for the finer grid, 1.243 for the coarser grid, and $C_{L\mathrm{rms}}$ was found to be 0.185 for both grids. The difference in dimensionless time values in Fig. 4(a) and (b) is due to the different methods used for making the time t dimensionless (using cylinder radius for Lu and Dalton, and here using cylinder diameter).

Forced in-line oscillation of a circular cylinder was investigated by Al-Mdallal et al. (2007) at $\mathrm{Re} = 200$, with a displacement of amplitude-to-cylinder diameter of $A_x = 0.1$ or 0.3 and in a wide frequency range of $f/\mathrm{St}_0 = 0.5$–3.0, where $\mathrm{St}_0 = 0.195$. Their method of solution is based on a conjugated Fourier spectral analysis with finite difference approximations. To validate the present code for in-line oscillation, computations were carried out for $\mathrm{Re} = 200$, $A_x = 0.1$, $f/\mathrm{St}_0 = 0.55$, 1.0, 1.45, 1.5, 1.75, 1.95, 2.2, and 2.8. Results for four frequency ratios are shown here in Figs. 5 and 6; the frequency ratios are as follows: (a) 1.5, (b) 1.75, (c) 1.95, and (d) 2.2. The left-hand side of the figures shows the time-histories of lift and of cylinder displacement (somewhat magnified), while the right-hand side gives Lissajous patterns for lift and nondimensional cylinder displacement. Note that in Fig. 5, the time-history is shown between $t = 0$ and 60, while in Fig. 6, $t = 240$–300 was chosen in order to capture lock-in (although in (d) it was not yet full). If full lock-in is obtained, the Lissajous curves become limit cycle curves. As can be seen, quite reasonable agreement has been obtained between the two sets of results. Similar agreement was found for the cases not shown here.

3. Orbital motion

Fig. 7 shows the flow arrangement for an orbiting cylinder. The orbital motion of the cylinder is created by the superposition of two forced oscillations with identical frequencies. The motion of the centre of the cylinder with unit diameter is specified as follows:

$$x_0(t) = A_x \cos(2\pi f_x t), \qquad y_0(t) = A_y \sin(2\pi f_y t). \tag{18}$$

Here $f_x = f_y = f$ for which nonzero A_x and A_y amplitudes gives an ellipse, shown in the dotted line in Fig. 7. A_x alone yields pure in-line oscillation, and then as A_y is increased, the ellipticity $e = A_y/A_x$ increases to yield a full circle at $e = 1$. Eq. (18) makes the cylinder orbit anticlockwise (counterclockwise); by changing the sign of y_0 in Eq. (18), a clockwise orbit is obtained. Later in this paper, the effect of orbital direction and that of the initial condition are investigated.

During each set of computations, Re and A_x are fixed, and f_x and f_y are kept constant at 85% or 90% of the frequency of vortex shedding from a stationary cylinder case denoted by St_0. The predicted values for St_0 at $\mathrm{Re} = 120$, 160, 180 are 0.1751, 0.1882, 0.1930, respectively (Baranyi and Lewis, 2006), and they are calculated using the power spectral density of the lift coefficient for the case of uniform flow past a stationary cylinder. The $f_x = f_y = f$ values were chosen to be near to the value of St_0 to ensure lock-in (synchronisation of vortex shedding frequency with that of the cylinder oscillation) at moderate oscillation amplitudes.

Computational results for orbital motion were compared with those of Didier and Borges (2008), who used a fully coupled finite volume method for computing flow around a cylinder forced to move along a circular path at $\mathrm{Re} = 300$. The maximum cylinder velocity components were identical and were set at 10% of the free-stream velocity U. The frequency ratio of forced oscillation f/St_0 was varied from 0.1 to 2.9. Since the cylinder velocity is obtained as a product of frequency and amplitude, a change in frequency caused the amplitude of cylinder motion to change inversely. To compare results, I carried out computations for a cylinder in circular orbit over the frequency ratio range of 0.5–2.8, for Strouhal number, $C_{D\mathrm{mean}}$, and the rms of lift and drag. Strouhal number curves versus frequency ratio for both methods are shown in Fig. 8. Both methods captured lock-in in the frequency ratio ranges of around 0.92–1.0 and 1.65–2.13, and the curves are in general agreement. The TMV of drag is shown in Fig. 9. The present method predicts slightly higher drag coefficient values (see Fig. 9(b)); however, agreement was good—surprisingly good, considering the difficulty in

determining the TMV and rms values outside the lock-in domain, where the signals tend to be quite irregular—and the curves follow a very similar tendency throughout the frequency ratio domain. Similar agreement was found in the curves of rms values of lift and drag (not shown here).

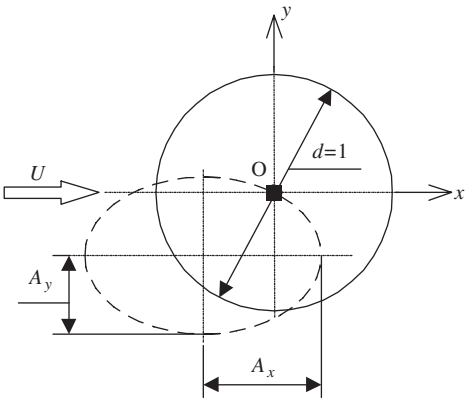

Fig. 7. Layout for the orbital path of the cylinder.

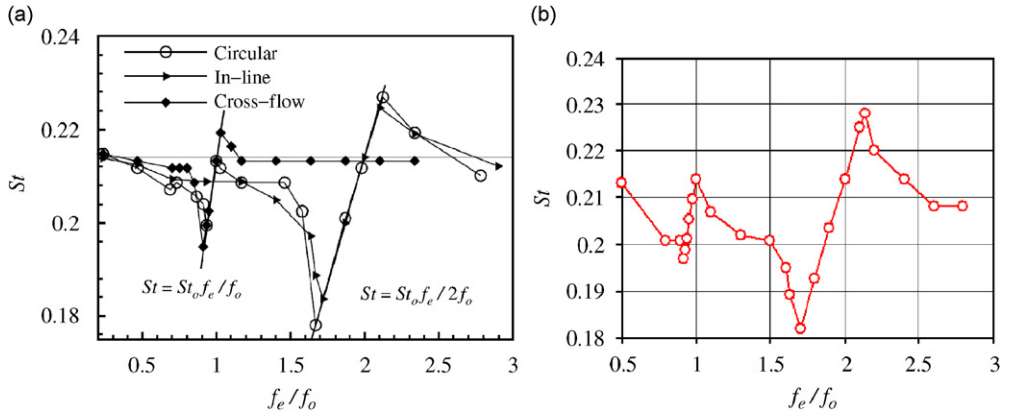

Fig. 8. Strouhal number versus frequency ratio for a cylinder in circular orbit (Re = 300, $A_x = A_y$, $St_0 = 0.214$), comparing (a) Didier and Borges (2008) and (b) Baranyi (circular orbit) (by permission of the publisher).

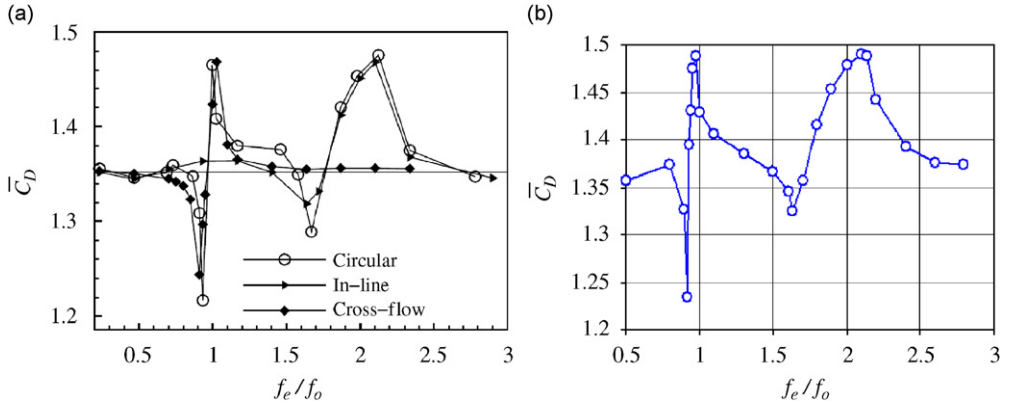

Fig. 9. Time-mean drag versus frequency ratio for a cylinder in circular orbit (Re = 300, $A_x = A_y$, $St_0 = 0.214$), comparing (a) Didier and Borges (2008) and (b) Baranyi (circular orbit) (by permission of the publisher).

Now that it has been shown that the results obtained by the code compare well with computational results for orbital cylinder motion as well as for stationary and oscillating cylinders, we investigate the effect of ellipticity on the force coefficients. An interesting phenomenon was observed when looking at the TMV (also denoted by an overbar) and rms values of the lift, drag and base pressure coefficients for an orbiting cylinder in a uniform flow. Abrupt jumps were found when these values were plotted against ellipticity e with Re and A_x kept constant (Baranyi, 2005a). A typical example for the TMV of the lift coefficient $\bar{C}_L$ is shown in Fig. 10 (here $\mathrm{Re} = 120$, $A_x = 0.4$, $f = 0.85\mathrm{St}_0$ where $\mathrm{St}_0 = 0.1751$, anticlockwise orbit), where three sudden jumps in the curve can be seen. Both upper and lower curves are almost straight lines and in general their slopes are almost identical. Two different states were found on the curve of $\bar{C}_L$ versus e, one with greater lift, and the other with smaller. Both show an approximately linear decrease with increasing e,

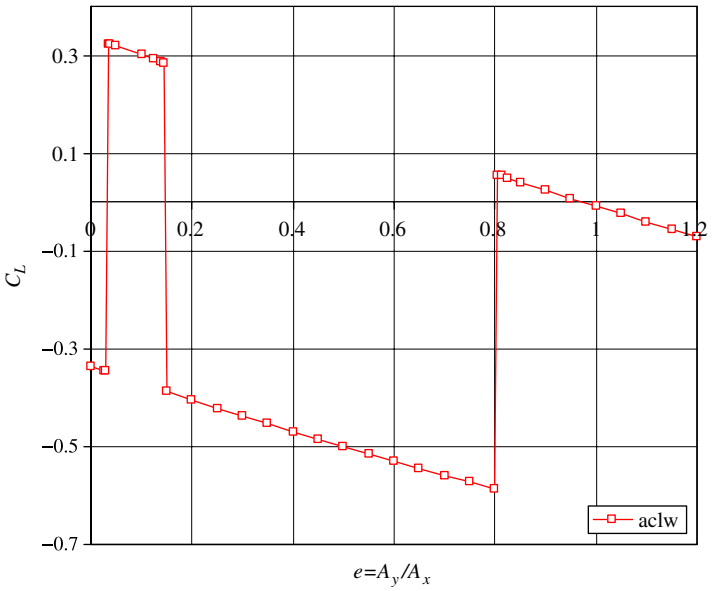

Fig. 10. Time-mean value of lift coefficient versus ellipticity ($\mathrm{Re} = 120$, $A_x = 0.4$, $f = 0.85\mathrm{St}_0$, $\mathrm{St}_0 = 0.1751$, anticlockwise (aclw) orbit).

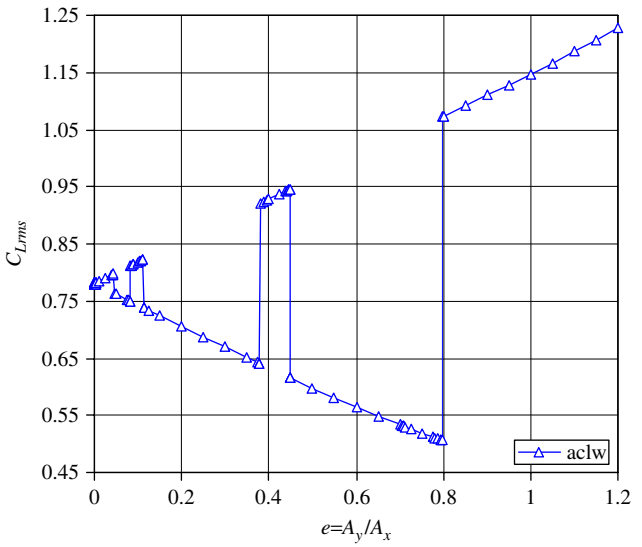

Fig. 11. Root-mean-square value of lift coefficient versus ellipticity ($\mathrm{Re} = 160$, $A_x = 0.4$, $f = 0.85\mathrm{St}_0$, $\mathrm{St}_0 = 0.1882$, anticlockwise (aclw) orbit).

and the difference between the $\bar{C}_L$ values belonging to the two states is approximately constant. It was shown in Baranyi (2004a, b) that the time histories of C_L before and after the jumps are substantially different.

The TMV and rms of drag and base pressure, further the rms of lift, behaved differently from $\bar{C}_L$, characterised by two state or envelope curves which are not parallel but intersect each other at $e = 0$. A typical example is shown in Fig. 11 ($\mathrm{Re} = 160$, $A_x = 0.3, f = 0.85\mathrm{St}_0$, where $\mathrm{St}_0 = 0.1882$, anticlockwise orbit). Further details about the jumps, the state curves, and the effect of Reynolds number and oscillation amplitude A_x can be found in Baranyi (2004a, b, 2005a, 2006). In addition, Lewis (2006), using the vortex cloud method, was able to reproduce three of the cases reported in Baranyi (2004a), finding jumps in the TMV and rms of lift and drag, plotted against the amplitude of transverse oscillation. Lewis' results lend support to the findings here, which indicate that there are two states, or two solutions and the solution jumps from one state to the other and back. It appears that these sudden changes in the time-mean and rms lift and other coefficients are the symptoms of sudden change in the vortex structure. What triggers these changes is uncertain; probably there are two attractors (periodic orbits in this case), each with its 'basin of attraction', of this nonlinear system and the solution is attracted to one or the other of the attractors depending on the values of the parameters. Let us investigate whether energy transfer is affected by the changes in state.

4. Energy transfer

The mechanical energy transfer between fluid and a transversely oscillated cylinder was defined in Blackburn and Henderson (1999) and is here extended to encompass the bidirectional character of orbital motion. In this case, mechanical energy transfer (E) takes place in both transverse and in-line directions. E is determined when the flow is already periodic and hence (y_0, C_L) and (x_0, C_D) represent limit cycles. Energy transfer E is positive when work is done on the cylinder and negative when work is done on the fluid by the cylinder.

Extending Blackburn and Henderson (1999)'s definition of E (mechanical energy transferred from the fluid to the moving cylinder per motion cycle), E can be written as follows:

$$E = \frac{2}{\rho U^2 d^2}\int_0^T \mathbf{F}\cdot\mathbf{v}_0\,\mathrm{d}t = \frac{2}{\rho U^2 d^2}\int_0^T (F_D v_{0x} + F_L v_{0y})\,\mathrm{d}t = \int_0^T (C_D\dot{x}_0 + C_L\dot{y}_0)\,\mathrm{d}t = E_2 + E_1, \tag{19}$$

where T is the motion period, x_0 and y_0 represent the dimensionless displacement of the cylinder in the x- and y-directions, respectively, and the overdot means differentiation by dimensionless time. Naturally, everything is dimensionless in the final integral in Eq. (19). As can be seen, the energy transfer can be divided into two parts, E_1 and E_2. Using Green's theorem E_1 can be written, for example, as:

$$E_1 = \int_0^T C_L(t)\dot{y}_0(t)\,\mathrm{d}t = \oint C_L\,\mathrm{d}y_0 = -\oint y_0\,\mathrm{d}C_L = \frac{1}{2}\left(\oint C_L\,\mathrm{d}y_0 - \oint y_0\,\mathrm{d}C_L\right).$$

Here line integrals are to be taken in clockwise direction. Similarly the energy transfer in the in-line direction is

$$E_2 = \int_0^T C_D(t)\dot{x}_0(t)\,\mathrm{d}t = \oint C_D\,\mathrm{d}x_0 = -\oint x_0\,\mathrm{d}C_D = \frac{1}{2}\left(\oint C_D\,\mathrm{d}x_0 - \oint x_0\,\mathrm{d}C_D\right).$$

The geometrical meaning of E_1 and E_2 is the signed area enclosed by limit cycles (y_0, C_L) and (x_0, C_D), respectively. E_1 and E_2 are positive when the orientation of the limit cycle curves is anticlockwise. Based on Eq. (19), the total energy transfer between fluid and cylinder is

$$E = E_2 + E_1.$$

5. Computational results and discussion

Computations were repeated for five different cases at $0.9\mathrm{St}_0$: $A_x = 0.4$ for $\mathrm{Re} = 120$ and 140; $A_x = 0.2$ and 0.3 for $\mathrm{Re} = 160$; and $A_x = 0.3$ for $\mathrm{Re} = 180$. Here, results are mainly given for the case of $\mathrm{Re} = 160$, as it generally represents other Re cases considered in this study.

5.1. Energy transfer results

Here, one set of results will be shown for the case of both clockwise and anticlockwise orbits at $\mathrm{Re} = 160$, $A_x = 0.3$, and $f = 0.9\mathrm{St}_0 = 0.16938$, where St_0 is the Strouhal number for a stationary cylinder at the given Re. The ellipticity e

was fixed for a single computation, then reset to a new e value for the next, to cover regularly and fairly densely the ellipticity domain from 0 (pure in-line oscillation) to 1.2 (past a full circle). The reason for this was to be able to identify any jumps occurring in the domain. When a sudden change occurred, several additional computations were performed on either side of the jump. The initial condition for both orbital directions was set at x_0 $(t=0)=A_x$, y_0 $(t=0)=0$ (3 o'clock position). The data shown here is representative of the several sets of computations performed.

Fig. 12 shows the mechanical energy variation with ellipticity for the parameters given above, for a clockwise direction of orbit. Here we can see energy transfer between the fluid and the body in the transverse direction E_1 (shown by empty squares). Note that E_1 values are positive for the upper state curve, meaning that energy is transferred from the fluid into the cylinder, and negative for the lower curve, with the energy transfer reversed, acting to dampen the motion. The energy transfer in the in-line direction E_2 (shown by empty diamonds) consists of two state curves, and all values are negative for both the upper and lower curves. This means that the force acting on the cylinder from the fluid would oppose the cylinder motion if it were not mechanically forced motion. Compared with E_1, the jumps occur at the same values of e, and the shape of the state curves is more or less reversed. Since the jumps are caused by the same sudden change in the vortex structure, the location of the jumps for one set of parameters is identical for all time-mean and rms values. The filled triangle signs represent the sum of the energy transfer in transverse and in-line directions $E=E_1+E_2$. The shape is that of E_1 but, like E_2, all of the values are negative, and thus the energy transfer for an orbiting cylinder was found to be always negative in the ellipticity domain investigated. The work, therefore, is done on the fluid by the cylinder, and naturally the fluid produces a kind of resistance against the forced motion of the cylinder. Computations were repeated for the anticlockwise direction of orbit, and identical curves to those of the clockwise orbit were obtained for E_1, E_2 and the sum of these two.

Next we will take a closer look at the jumps. This has been done by investigating the time-history lift coefficient curves [see Baranyi (2004a)], where it was found that the shape of the signals before and after a jump was substantially different, leading to different time-mean and rms values of lift. Here, the limit cycles are investigated before and after a jump, for a clockwise orbit at the parameters given at the beginning of this subsection. The jump investigated was at about $e=0.1435$ (see, for instance, Fig. 12). Fig. 13 shows the two limit cycles (y_0, C_L) in periodic flow representing the transverse cylinder motion component of an anticlockwise orbit. The limit cycle for the e value before the jump, $e=0.143$ $(A_y=0.0429)$, is shown by the thinner line. The thicker line represents the limit cycle just after the jump, at $e=0.144$ $(A_y=0.0432)$. Although the e values hardly differ, the two limit cycle curves are completely different, almost reflecting each other, and with a change in orientation of traverse around the limit cycles. This means that the sign of energy transfer is opposite for the two curves: negative for $e=0.143$ $(E_1=-0.0521)$ and positive for $e=0.144$ $(E_1=0.0491)$. This finding is very similar to that of Blackburn and Henderson (1999) and Blackburn (2003) for a transversely oscillated cylinder with varying oscillation frequency. They also found a change in the orientation of the limit cycles, indicating a sign change in energy transfer. Although orbital motion is different from pure transverse motion, since the reflection symmetry is destroyed, there is some similarity in that the solution can be very sensitive to even a small change in A_y, which can lead to a dramatic change in the limit cycle curves (y_0, C_L) and in the sign of E_1, i.e., energy transfer between the cylinder and the fluid in the transverse direction.

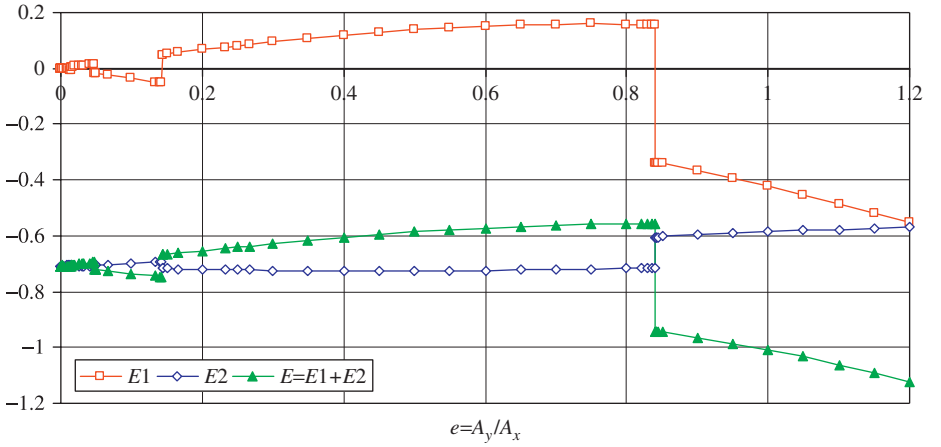

Fig. 12. Energy transfer coefficients E_1, E_2 and E versus ellipticity (Re = 160, $A_x=0.3$; $f=0.9\mathrm{St}_0$, $\mathrm{St}_0=0.1882$, clockwise orbit).

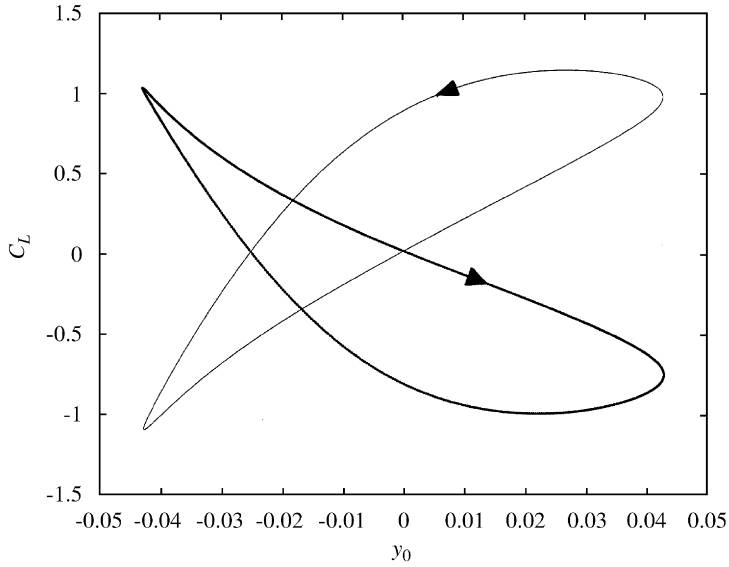

Fig. 13. Limit cycles (y_0, C_L) (thin line: $A_y = 0.0429$; thick line:$A_y = 0.0432$) (Re = 160, $A_x = 0.3$, $f = 0.9\mathrm{St}_0$, $\mathrm{St}_0 = 0.1882$, clockwise orbit).

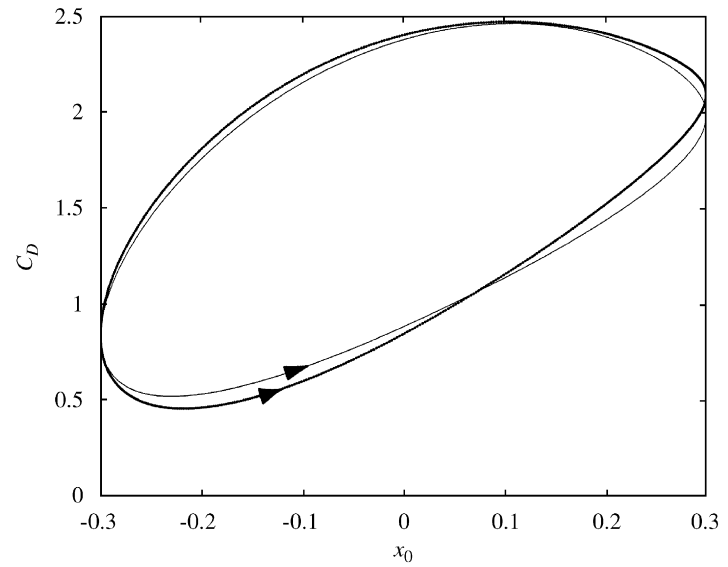

Fig. 14. Limit cycles (x_0, C_D) (thin line: $A_y = 0.0429$; thick line: $A_y = 0.0432$) (Re = 160, $A_x = 0.3$, $f = 0.9\mathrm{St}_0$, $\mathrm{St}_0 = 0.1882$, clockwise orbit).

Fig. 14 shows the two limit cycles (x_0, C_D) in periodic flow representing the in-line cylinder motion component of an anticlockwise orbit. Again the limit cycle for the e value before the jump, at $e = 0.143$ ($A_y = 0.0429$), is shown by the thinner line. The thicker line represents the limit cycle just after the jump, at $e = 0.144$ ($A_y = 0.0432$). As can be seen in this figure, in contrast with the results shown in Fig. 13, the small change in the value of ellipticity did not cause any drastic change in the two limit cycle curves. The shape of the curves is almost the same and their orientation is identical. This orientation means negative energy transfer values: $E_2 = -0.6947$ for $e = 0.143$ and $E_2 = -0.7663$ for $e = 0.144$. As can be seen, the absolute value of E_2 is much larger than that of E_1 with the same e values, so that the overall energy transfer E, i.e., the sum of E_1 and E_2, is negative for both of these cases.

Interestingly, the limit cycle for transverse displacement changes radically with a tiny change in ellipticity, but the limit cycle for in-line motion hardly changes at all. This means that the limit cycle for the lift coefficient and

nondimensional transverse displacement is much more sensitive to the trigger for the jumps than is the limit cycle based on the drag coefficient and in-line displacement. This result suggests that lift and drag will behave differently in other measures of examining the jump phenomenon, such as phase angle analysis.

5.2. Phase angle results and flow patterns

Several studies, all for transversely oscillated cylinders [see e.g. Lu and Dalton (1996) for Re = 185, 500, and 1000; Blackburn and Henderson (1999) for Re = 500; Blackburn (2003)] also for Re = 500), have shown a sudden shift occurring in the phase angle under lock-in condition when the cylinder oscillation frequency at a given Reynolds number is in the vicinity of the vortex shedding frequency from a stationary cylinder at that Re. Because of this, it seemed worthwhile to investigate the phase angle Φ_L between the lift coefficient and displacement of the cylinder in transverse direction.

The phase angle Φ_L is defined for clockwise and anticlockwise cylinder orbit in the sense of

$$\text{clockwise}: y_0 = -A_y \sin(2\pi ft); \quad C_L \approx -A_L \sin(2\pi ft + \Phi_L),$$

$$\text{anticlockwise}: y_0 = A_y \sin(2\pi ft); \quad C_L \approx A_L \sin(2\pi ft + \Phi_L),$$

where A_L is the amplitude of lift coefficient.

Fig. 15 shows that there is indeed a drastic change in the phase angle Φ_L. The solid line, with a sine wave with the amplitude of 1.5, represents the time-history of transverse cylinder displacement. The amplitude, which is considerably smaller in reality, has been exaggerated here to provide a convenient means to visualise the phase angle. The dotted line is the lift coefficient at $A_y = 0.0429$ ($e = 0.143$), prior to the jump, while the heaviest line (composed of crosses) is the lift at $A_y = 0.0432$ ($e = 0.144$), after the jump. The pre-jump curve is basically in phase with the cylinder displacement, while the post-jump curve is essentially reversed, yielding a phase shift of about 180°. Thus, the jump has created a sudden change in the phase angle of about 180° for lift.

The effect of the jump on the phase angle between drag and in-line cylinder displacement, on the other hand, is almost negligible, as seen in Fig. 16. The solid line again represents the time-history of displacement. The two hardly distinguishable lines are the pre-jump drag coefficient at $A_y = 0.0429$ (dotted line) and the post-jump drag at $A_y = 0.0432$ (the heaviest line).

These findings suggest that any follow-up investigation should focus on the phase angle between lift and transverse displacement. Therefore, for the representative case (Re = 160, $A_x = 0.3$, $f = 0.9\mathrm{St}_0 = 0.16938$), Φ_L is determined and plotted versus ellipticity in Fig. 17 for both clockwise (empty square) and anticlockwise (filled triangle) directions of orbit. The two curves practically coincide, showing that phase angle is insensitive to the direction of orbit. The two curves have jumps at the same location as for the other curves (e.g., in Fig. 12). Comparing Figs. 12 and 17, it can be observed that when the energy transfer in the transverse direction $E_1 > 0$, then the phase angle is $\Phi_L \simeq 180°$, and when it is negative, then $\Phi_L \simeq 0°$. This 180° phase shift through the jumps is in agreement with the findings of Lu and Dalton (1996), Blackburn and Henderson (1999) and Blackburn (2003).

One hypothesis for the sudden changes in phase angle in the case of a transversely oscillated cylinder is that the change in flow structure results from a change in balance between two different vorticity production mechanisms, as proposed by Blackburn and Henderson (1999) and Blackburn (2003). They investigated forced transverse cylinder oscillation at Re = 500 and a nondimensional amplitude of oscillation of 0.25, while changing the frequency ratio near the natural shedding frequency (0.75–1.05). Switches in phase angles and flow patterns were found when comparing results for frequency ratios of 0.875 and 0.975. They suggest that the switches are due to competition between two vorticity production mechanisms. This hypothesis seems to be a likely explanation for the switching phenomenon found here for orbiting cylinders.

Fig. 18 displays computed flow patterns showing near-wake streamlines at cylinder positions in 30° steps in the polar angle Θ for a clockwise orbit at two ellipticity values (pre- and post-jump, for the same jump as in, e.g., Figs. 12–17). A vertical view of the flow patterns shows the development of vortices at the two ellipticity values given. The flow patterns, when viewed in horizontal pairs, illustrate the fact that the timing of the vortex shedding is changed dramatically by a very small change in the ellipticity (from $e = 0.143$ to 0.144), to almost a mirror image of each other. These sudden changes in the flow pattern are similar to those found by Blackburn (2003) when he altered the frequency of transverse cylinder oscillation. He plotted vorticity contours at a point of maximum cylinder displacement for two frequency ratios, one below and the other above a critical frequency ratio belonging to a switch. Flow patterns represented by vorticity contours were substantially different in the two cases and also the energy transfer between the cylinder and fluid per motion cycle was of the opposite sign for the two cases (Blackburn, 2003). Both of these features are found in the present study when considering flows around an orbiting cylinder

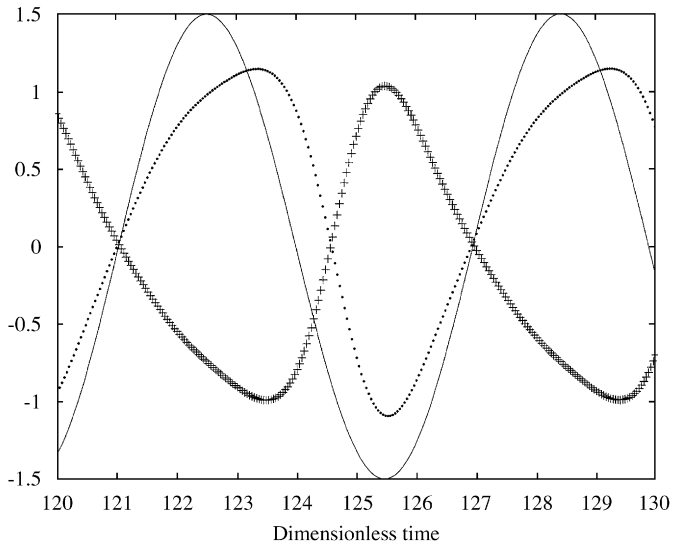

Fig. 15. Time histories of lift coefficient and cylinder displacement (solid line: transverse cylinder displacement; dotted line: C_L at $A_y = 0.0429$; +line:C_L at $A_y = 0.0432$) (Re = 160, $A_x = 0.3$, $f = 0.9\mathrm{St}_0$, $\mathrm{St}_0 = 0.1882$, clockwise orbit).

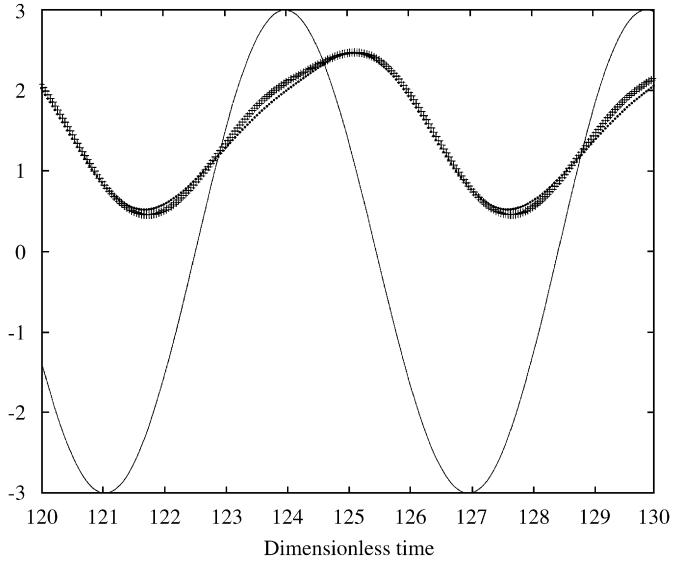

Fig. 16. Time histories of drag coefficient and cylinder displacement (solid line: in-line cylinder displacement; dotted line: C_D at $A_y = 0.0429$; +line: C_D at $A_y = 0.0432$) (Re = 160, $A_x = 0.3$, $f = 0.9\mathrm{St}_0$, $\mathrm{St}_0 = 0.1882$, clockwise orbit).

with ellipticity below and above the critical ellipticity value. It seems likely that the small change in ellipticity has caused the boundary between two basins of attraction of this nonlinear system to be crossed, leading to a switch in flow pattern.

5.3. Effect of orbital direction

Here, one set of results will be shown for the case of both clockwise and anticlockwise orbits at Re = 160, $A_x = 0.3$, and $f = 0.9\mathrm{St}_0$, where St_0 is the Strouhal number for a stationary cylinder at Re = 160 (i.e., $\mathrm{St}_0 = 0.1882$). This set is representative of the several sets of computations performed.

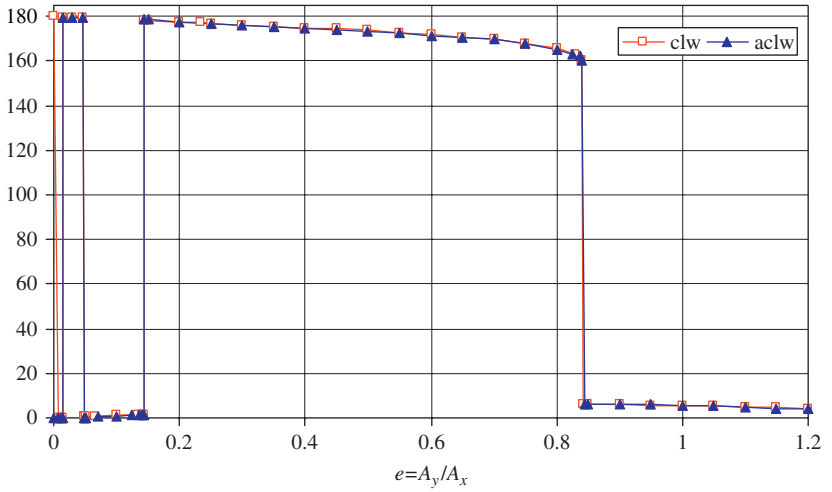

Fig. 17. Phase angle (in degrees) versus ellipticity for clockwise (clw) and anticlockwise (aclw) cylinder orbit (Re = 160, $A_x = 0.3$, $f = 0.9\mathrm{St}_0$, $\mathrm{St}_0 = 0.1882$).

Fig. 19 gives $\bar{C}_L$ versus ellipticity e. The filled triangles show results for a cylinder orbiting anticlockwise (aclw in the figure). Note that there are two state curves that are roughly parallel with each other and of negative slope, as seen earlier in Fig. 10. The empty squares in Fig. 19 show results for a clockwise (clw) orbit, with the other parameters unchanged. The two state curves can be seen, again roughly parallel, but the slope is positive, and they form a mirror image of the state curves of the cylinder orbiting anticlockwise. There are four jumps or switches in state, although this is difficult to identify at this scale; there is therefore no change in jump location with orbital direction. In all computations done so far, $\bar{C}_L$ has shown this pattern: a mirror image of each other, with the slope of the anticlockwise curve being negative and that of the clockwise curve positive.

Unlike $\bar{C}_L$, the other TVM and all of the rms values investigated, when plotted against ellipticity, are basically unaffected by the direction of orbit. Fig. 20 gives the curves for $C_{pb\mathrm{rms}}$ as a representative of this group (in which state curves intersect at zero ellipticity). Results for the clockwise and anticlockwise direction of orbit fall on the same state curves and jump locations, so that it is difficult to distinguish the two curves.

From the sets of computations for the two orbital directions, it is clear that two pairs of state curves exist and fall into two different categories: for $\bar{C}_L$, the state curves are roughly parallel, and for the rest the curves intersect at zero. This is reassuring in two ways: (i) the code produces the same time-mean and rms results for two different situations represented by the two directions of orbit, and this confirms that the code is reliable, and (ii) results obtained for two different cases strengthen the hypothesis of the existence of two solutions, or two basins of attraction.

Apart from the TMV of lift, it was found that the direction of orbit has basically no effect on time-mean and rms values of the force coefficients. However, it may be worth noting that since $\bar{C}_L$ is affected, it may be necessary to take the direction of orbit into consideration when using results from orbital studies, most of which are carried out using only one orbital direction.

5.4. *Effect of initial condition*

Here we examine the effect of initial condition, or what happens when a cylinder is started from a different position along its path. Let us write the cylinder motion in the following forms:

$$x_0(t) = A_x \cos(2\pi ft + \Theta), \qquad y_0(t) = -A_y \sin(2\pi ft + \Theta),$$

where Θ is a polar angle measured clockwise from positive x-axis, representing the initial position of the centre of the cylinder. For earlier clockwise computations, the initial conditions were $x_0\,(t=0) = A_x$, $y_0\,(t=0) = 0$ (i.e., $\Theta = 0^\circ$; 3 o'clock position) for the standard case in this paper (Re = 160; $A_x = 0.3$; $f = 0.9\mathrm{St}_0 = 0.16938$). The computations were repeated for a clockwise orbit using a different initial condition $x_0\,(t=0) = -A_x$, $y_0\,(t=0) = 0$ (i.e., $\Theta = 180^\circ$; 9 o'clock position).

Figs. 21 and 22 give two representative state curves, for $\bar{C}_L$ (where the two state curves are almost parallel with each other) and for E_1 (where the state curves intersect at zero ellipticity), respectively. The two pairs of $\bar{C}_L$ state curves in Fig. 21 are identical, in contrast with Fig. 19, where the change in orbital direction caused the state curves to switch

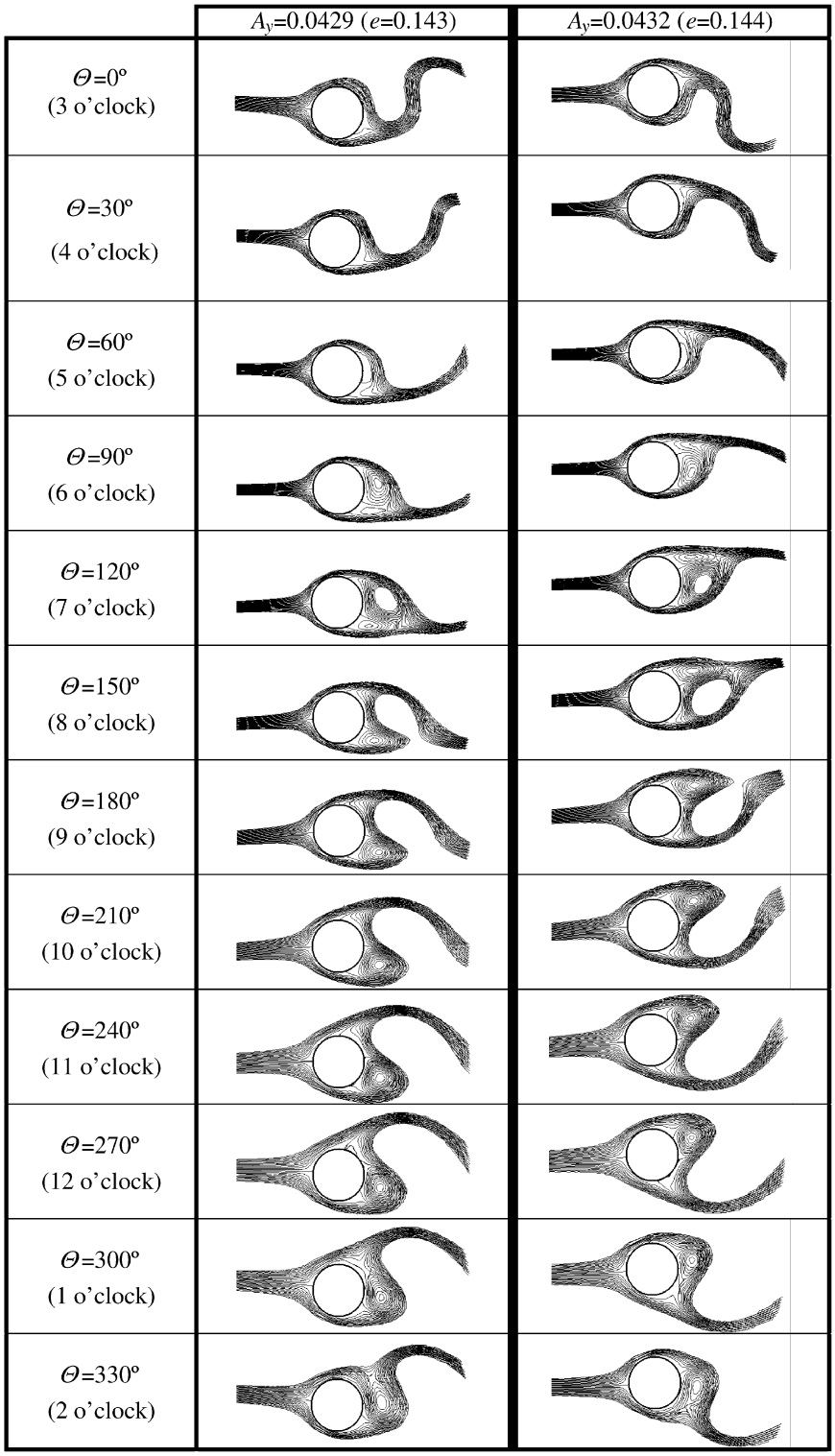

Fig. 18. Flow patterns for $A_y = 0.0429$ (left-hand column) and $A_y = 0.0432$ (right-hand column) at equidistant cylinder positions Θ ($\mathrm{Re} = 160$, $A_x = 0.3$, $f = 0.9\mathrm{St}_0$, $\mathrm{St}_0 = 0.1882$, clockwise orbit).

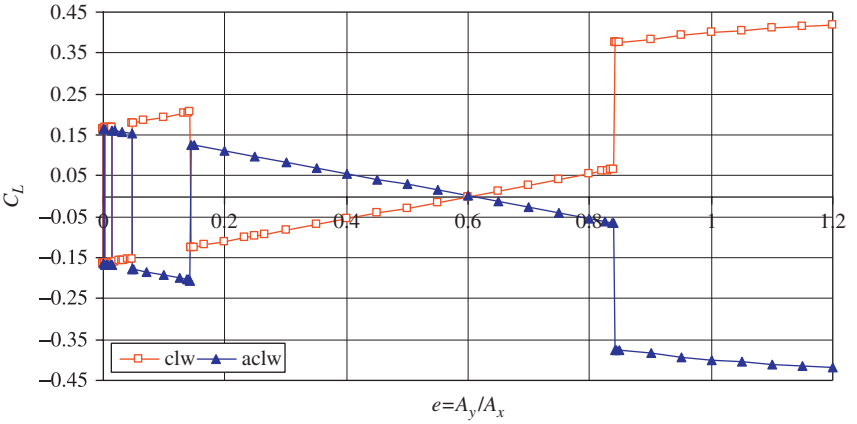

Fig. 19. Time-mean value of lift coefficient versus ellipticity for clockwise (clw) and anticlockwise (aclw) cylinder orbit (Re = 160, $A_x = 0.3$, $f = 0.9\mathrm{St}_0$, $\mathrm{St}_0 = 0.1882$).

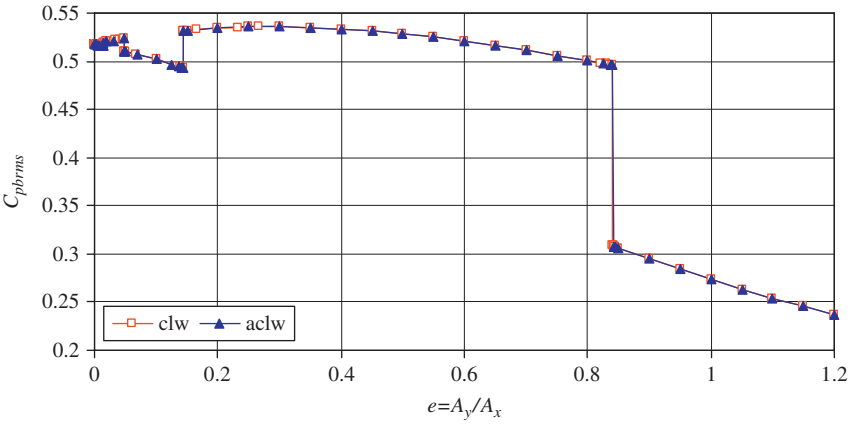

Fig. 20. Root-mean-square value of base pressure coefficient versus ellipticity for clockwise (clw) and anticlockwise (aclw) cylinder orbit (Re = 160, $A_x = 0.3$, $f = 0.9\mathrm{St}_0$, $\mathrm{St}_0 = 0.1882$).

slope. The initial condition, however, affects the location of jumps between the two state curves. The E_1 state curves in Fig. 22 show basically the same features, in that the two pairs of state curves are identical, and the change in initial condition changes the location of jumps (this can perhaps be more easily seen by comparing the E_1 curve in Fig. 12 with the $\Theta = 180^\circ$ curve in Fig. 22). If Figs. 21 and 22 are compared, it is evident that the location of jumps is identical for the $\tilde{C}_L$ and E_1 curves at each initial condition, and this correspondence is true for every force coefficient investigated, as well as for the energy transfer per motion cycle.

It is interesting that, although the state curves are identical, shifting the starting point of calculations has changed the location of the jumps. For all five sets of computations at different Re and A_x, specified at the beginning of this section, exactly the same type of results were obtained. For each set of variables (the TMV and rms of C_L, C_D and C_{pb}, and the mechanical energy transfer E_1, E_2 and E), the location of jumps for the same initial condition was always the same. Unlike a change in orbital direction, a change in the initial conditions prompts an alteration in the ellipticity value at which the switch in the vortex structure takes place. Thus, we have established that a change in any one parameter in a set of five parameters (Re, A_x, e, f and initial cylinder position Θ) can influence the attractor to which the solution is attracted.

Computations were repeated for different initial conditions for the same case, also in clockwise orbit. It was found that with only three different initial cylinder positions of $\Theta = 60^\circ$, 90° and 180° (corresponding to 5, 6 and 9 o'clock cylinder positions, respectively) the two state curves can be almost fully reproduced in the rms values or TMV of lift, drag and base pressure coefficients versus ellipticity e plane. Fig. 23 shows this for the TMV of the lift coefficient. If we check the figure more carefully, we can see that there is a small interval at $e = 0.258$–0.275 (see Fig. 24, the zoomed-out

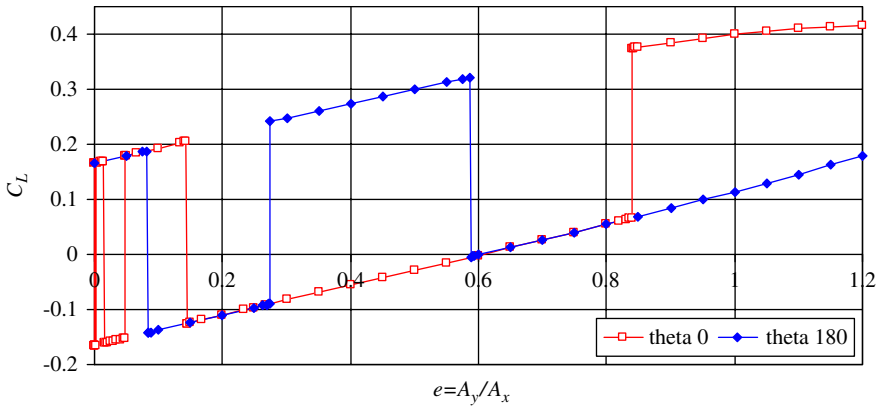

Fig. 21. Time-mean value of lift coefficient versus ellipticity: effect of initial condition ($\Theta = 0^\circ$ and 180°), (Re = 160, $A_x = 0.3$, $f = 0.9\mathrm{St}_0$, $\mathrm{St}_0 = 0.1882$, clockwise orbit).

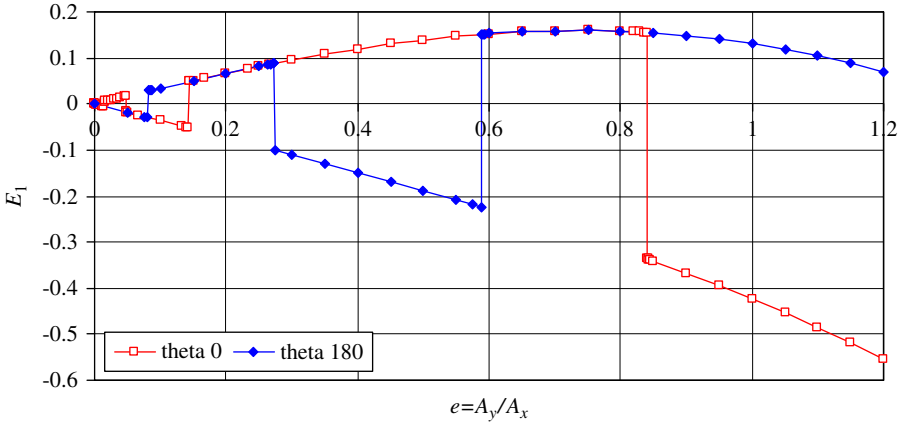

Fig. 22. Transverse energy transfer E_1 versus ellipticity: effect of initial condition ($\Theta = 0^\circ$ and 180°) (Re = 160, $A_x = 0.3$, $f = 0.9\mathrm{St}_0$, $\mathrm{St}_0 = 0.1882$, clockwise orbit).

version of Fig. 23), where only the lower state curve is fully realised. The length of the gap in the upper state curve is about 1.4% of the domain of e investigated here (0–1.2).

Although additional computations were done at several different Θ values, interestingly, none of them were able to realise the upper state curve in the critical $e = 0.258$–0.275 domain. Further investigation may reveal an appropriate value, or find an explanation for this curious gap. The very fact that the gap exists suggests the complexity of the boundaries between the basins of attraction. It may be that with this combination of parameters (Re, A_x, f/St_0) in the critical e domain, only the solution belonging to the lower state curve can be reached.

6. Conclusions

The present study deals with an orbiting cylinder, in forced motion, placed in a uniform flow at low Reynolds numbers (Re = 120–180). The objective of the paper was to investigate further the phenomenon of sudden changes in vortex structure that occur when the ellipticity of the orbital path is changed.

6.1. Energy transfer and phase angle

The definition of mechanical energy transfer between a transversely oscillated cylinder and fluid [see Blackburn and Henderson (1999)] was extended here for use with a cylinder mechanically forced to follow an orbital path. Energy

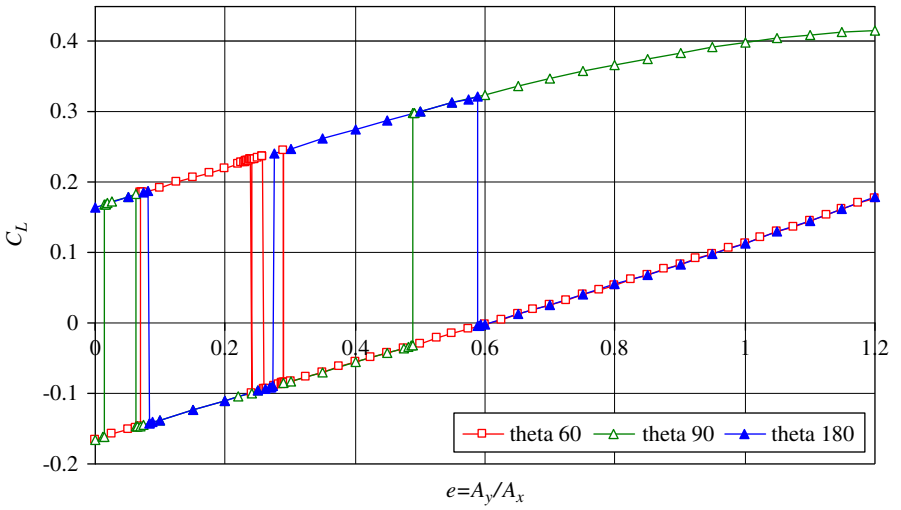

Fig. 23. Time-mean value of lift coefficient versus ellipticity: effect of initial condition ($\Theta = 60^\circ$, 90° and 180°), (Re = 160, $A_x = 0.3$, $f = 0.9\mathrm{St}_0$, $\mathrm{St}_0 = 0.1882$, clockwise orbit).

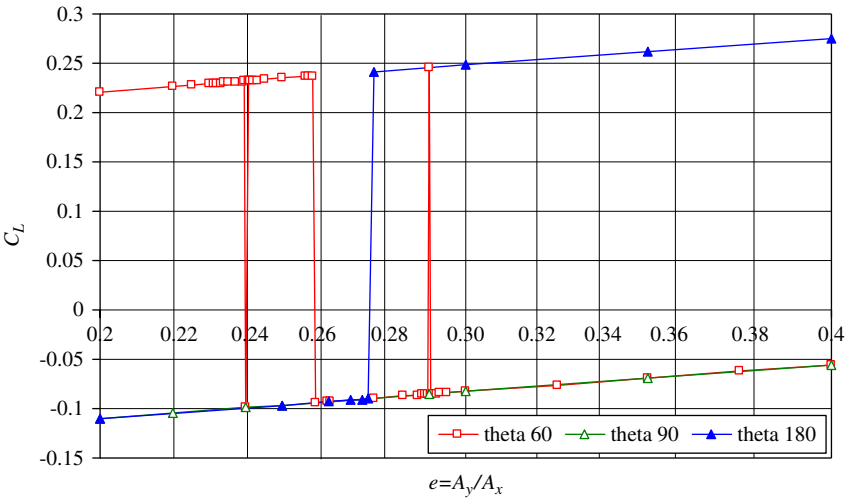

Fig. 24. Time-mean value of lift coefficient versus ellipticity, effect of initial condition ($\Theta = 60^\circ$, 90° and 180°; zoom in), (Re = 160, $A_x = 0.3$, $f = 0.9\mathrm{St}_0$, $\mathrm{St}_0 = 0.1882$, clockwise orbit).

transfer in this case is composed of two parts, E_1 for the energy transfer in the transverse direction, and E_2 for the in-line direction. These variables were investigated against different values of ellipticity. The overall energy transfer E is always negative, meaning that energy is transferred from the cylinder to the fluid. The sign of E_1 determines the magnitude of the phase angle between lift and transverse cylinder displacement (if positive, then phase angle $\Phi_L \approx 180^\circ$, if negative, $\Phi_L \approx 0^\circ$). The location of jumps in the Φ_L–e curve were identical to the location of jumps for time-mean and rms values and for energy transfer E_1, E_2 and E.

6.2. Limit cycles

Limit cycle curves were investigated immediately prior to and after a jump. The limit cycle for the transverse displacement and lift changes radically with a tiny change in ellipticity, but the limit cycle for the in-line motion and drag hardly changes at all. This shows that the limit cycle for the lift coefficient and nondimensional transverse

displacement is much more sensitive to the trigger for the jumps than is the limit cycle based on the in-line displacement and drag coefficient.

6.3. Flow patterns

Flow patterns for two ellipticity values around the full shedding cycle illustrate the development of near-wake vortices. Comparison of the two sets shows that the timing of the vortex shedding is changed dramatically to a near-mirror image by a very small change in the ellipticity (from $e = 0.143$ to 0.144).

6.4. Orbital direction

Clockwise and anticlockwise cylinder orbits were compared. From the sets of computations for the two orbital directions, it is clear the two pairs of state curves fall into two different categories: for the time-mean of lift, the state curves are roughly parallel, and the slope changes with orbital direction to a mirror image; while for the other, time-mean and rms values the curves intersect at zero ellipticity and do not change with the change in orbital direction. Apart from the time-mean of lift, it was found that the direction of orbit has basically no effect on the time-mean and rms values of the force coefficients. The location of the jumps was unaffected for all curves belonging to a given set of data.

6.5. Initial conditions

A change in initial cylinder position produces state curves that are identical, but changes the location of the jumps for all time-mean and rms values belonging to the same set of parameters investigated, and changes them to the same location for each of the cases. Since the jumps are caused by the same sudden change in the vortex structure, the location of the jumps for one set of parameters is identical for all time-mean and rms values. Unlike a change in orbital direction, a change in the initial condition prompts an alteration in the ellipticity value at which the switch in the vortex structure takes place. By changing the initial cylinder position while keeping all other parameters fixed, it may be possible to reach either the upper state curve or the lower; both solutions may therefore be attainable at the same ellipticity value.

This study confirms that two possible flow structures exist and shows that small changes in ellipticity or changes in initial conditions can cause a sudden switch in state. It seems that in the 'basins of attraction' there are two attractors in the form of periodic orbits, and a change in any one parameter in a set of five parameters (Reynolds number, amplitudes of in-line and transverse oscillation, frequency of cylinder oscillation, and initial cylinder position) can influence which attractor the solution is attracted to.

Acknowledgements

The support provided by the Hungarian Research Foundation (OTKA, Project no. T 042961) is gratefully acknowledged. The author also thanks Mr S. Ujvárosi for preparing several figures.

References

Al-Mdallal, Q.M., Kocabiyik, S., 2006. Rotational oscillations of a cylinder in cross-flow. International Journal of Computational Fluid Dynamics 20, 293–299.

Al-Mdallal, Q.M., Lawrence, K.P., Kocabiyik, S., 2007. Forced streamwise oscillations of a circular cylinder: locked-on modes and resulting fluid forces. Journal of Fluids and Structures 23, 681–701.

Anagnostopoulos, P., 1989. Numerical solution for laminar two-dimensional flow about a fixed and transversely oscillating cylinder in a uniform stream. Journal of Computational Physics 85, 434–456.

Baek, S.J., Sung, H.J., 2000. Quasi-periodicity in the wake of a rotationally oscillating cylinder. Journal of Fluid Mechanics 408, 275–300.

Baranyi, L., 2003. Computation of unsteady momentum and heat transfer from a fixed circular cylinder in laminar flow. Journal of Computational and Applied Mechanics 4 (1), 13–25.

Baranyi, L., 2004a. Numerical simulation of flow past a cylinder in orbital motion. Journal of Computational and Applied Mechanics 5 (2), 209–222.

Baranyi, L., 2004b. Sudden jumps in time-mean values of lift coefficient for a circular cylinder in orbital motion in a uniform flow. In: de Langre, E., Axisa, F. (Eds.), Proceedings of the 8th International Conference on Flow-Induced Vibration, Paris, vol. II, pp. 93–98.

Baranyi, L., 2005a. Abrupt changes in the root-mean-square values of force coefficients for an orbiting cylinder in uniform stream. In: Leweke, T., Williamson, C.H.K. (Eds.), Proceedings of the 4th Symposium on Bluff Body Wakes and Vortex-Induced Vibrations, Santorini, Greece, pp. 55–58.

Baranyi, L., 2005b. Lift and drag evaluation in translating and rotating non-inertial systems. Journal of Fluids and Structures 20, 25–34.

Baranyi, L., 2006. Energy transfer between an orbiting cylinder and moving fluid. In: Proceedings of PVP2006-ICPVT-11 ASME Pressure Vessels and Piping Division Conference, Vancouver, Canada, 2006, on CD ROM.

Baranyi, L., Lakatos, K., 2004. Computational fluid dynamics analysis of low Reynolds number flow around stationary and oscillating cylinders. In: Proceedings of the 4th International Engineering Conference, vol. 1, Mansoura-Sharm El-Shiekh, Egypt, pp. 459–465.

Baranyi, L., Lewis, R.I., 2006. Comparison of a grid-based CFD method and vortex dynamics predictions of low Reynolds number cylinder flows. The Aeronautical Journal 110 (1103), 63–71.

Baranyi, L., Shirakashi, M., 1999. Numerical solution for laminar unsteady flow about fixed and oscillating cylinders. Computer Assisted Mechanics and Engineering Sciences 6, 263–277.

Barkley, D., Henderson, R.D., 1996. Three-dimensional Floquet stability analysis of the wake of a circular cylinder. Journal of Fluid Mechanics 322, 215–241.

Bearman, P.W., Obasaju, E.D., 1982. An experimental study of pressure fluctuations on fixed and oscillating square-section cylinders. Journal of Fluid Mechanics 119, 297–321.

Bearman, P.W., Graham, J.M.R., Lin, X.W., Meneghini, J.R., 1995. Numerical simulation of flow-induced vibration of a circular cylinder in uniform and oscillatory flow. In: Bearman, P.W. (Ed.), Proceedings of the 6th International Conference on Flow-Induced Vibration, A.A. Balkema, Rotterdam, pp. 231–240.

Blackburn, H.M., Henderson, R.D., 1999. A study of two-dimensional flow past an oscillating cylinder. Journal of Fluid Mechanics 385, 255–286.

Blackburn, H.M., 2003. Computational bluff body fluid dynamics and aeroelasticity. In: Barton, N.G., Periaux, J. (Eds.), Coupling of Fluids, Structures and Waves Problems in Aeronautics, Notes on Numerical Fluid Mechanics and Multidisciplinary Design (NNFM), vol. 85. Springer, pp. 10–23.

Borthwick, A.G.L., 1986. Orbital flow past a cylinder: a numerical approach. International Journal for Numerical Methods in Fluids 6, 677–713.

Chakraborty, J., Verma, N., Chhabra, R.P., 2004. Wall effects in flow past a circular cylinder in a plane channel: a numerical study. Chemical Engineering and Processing 43, 1529–1537.

Chaplin, J.R., Subbiah, K., 1996. Wave and current loads on large scale horizontal cylinders. In: Proceedings of an International Conference in Ocean Engineering COE '96, ITT, Madras, India, pp. 199–209.

Chen, M.M., Dalton, C., Zhuang, L.X., 1995. Force on a circular cylinder in an elliptical orbital flow at low Keulegan-Carpenter numbers. Journal of Fluids and Structures 9, 617–638.

Dennis, S.C.R., Nguyen, P., Kocabiyik, S., 2000. The flow induced by a rotationally oscillating and translating circular cylinder. Journal of Fluid Mechanics 407, 123–144.

Didier, E., Borges, A.R.J., 2008. Numerical predictions of low Reynolds number flow over an oscillating circular cylinder. Journal of Computational and Applied Mechanics (in press).

Fletcher, C.A.J., 1997. , Second ed. Computational Techniques for Fluid Dynamics, vol. 2. Springer, Berlin.

Harlow, F.H., Welch, J.E., 1965. Numerical calculation of time-dependent viscous incompressible flow of fluid with free surface. Physics of Fluids 8, 2182–2189.

Kaiktsis, L., Triantafyllou, G.S., Özbas, M., 2004. Excitation and inertia forces on a cylinder vibrating transversely to a steady flow. In: de Langre, E., Axisa, F. (Eds.), Proceedings of the 8th International Conference on Flow-Induced Vibration, Paris, vol. II, pp. 463–467.

Kawamura, T., Kuwahara, K., 1984. Computation of high Reynolds number flow around a circular cylinder with surface roughness. In: Proceedings of the 22nd Aerospace Science Meeting, Reno, Nevada, AIAA-84-0340.

Kocabiyik, S., Nguyen, P., 1999. On a translating and transversely oscillating cylinder: Part 2: Effect of the velocity ratio on the hydrodynamic forces and the near-wake structure. Ocean Engineering 26, 21–45.

Koide, M., Tomida, S., Takahashi, T., Baranyi, L., Shirakashi, M., 2002. Influence of cross-sectional configuration on the synchronization of Kármán vortex shedding with the cylinder oscillation. JSME International Journal, Series B 45 (2), 249–258.

Kravchenko, A.G., Moin, P., Shariff, K., 1999. B-Spline method and zonal grids for simulations of complex turbulent flows. Journal of Computational Physics 151, 757–789.

Lewis, R.I., 2006. Application of vortex cloud flow modelling to cylinders in orbital motion at low Reynolds numbers and comparisons with some published grid-based CFD predictions. In: Lajos, T., Vad, J. (Eds.), Proceedings of the Conference on Modelling Fluid Flow, Budapest, vol. I, pp. 157–164.

Lu, X.Y., Dalton, C., 1996. Calculation of the timing of vortex formation from an oscillating cylinder. Journal of Fluids and Structures 10, 527–541.

Meneghini, J.R., Bearman, P.W., 1995. Numerical simulation of high amplitude oscillatory flow about a circular cylinder. Journal of Fluids and Structures 9, 435–455.

Mureithi, N.W., Rodriguez, M., 2005. Stability and bifurcation analysis of a forced cylinder wake. Paper IMECE2005-79778. In: Proceedings of the ASME International Mechanical Engineering Congress and Exhibition, Orlando, FL, USA, pp. 1–8.

Mureithi, N.W., Rodriguez, M., 2006. Cylinder wake dynamics in the presence of stream-wise harmonic forcing. Paper PVP2006-11-93847. In: Proceedings of the 2006 ASME Pressure Vessels and Piping Division Conference, Vancouver, BC, Canada.

Mureithi, N.W., Cotoi, I., Rodriguez, M., 2004. Response of the Karman wake to external periodic forcing and implications for vortex shedding control. In: de Langre, E., Axisa, F. (Eds.), Proceedings of the 8th International Conference on Flow-Induced Vibration, Paris, vol. I, pp. 87–92.

Norberg, C., 2003. Fluctuating lift on a circular cylinder: review and new measurements. Journal of Fluids and Structures 17, 57–96.

Öngören, A., Rockwell, D., 1988. Flow structure from an oscillating cylinder. Part 1. Mechanisms of phase shift and recovery in the near wake. Journal of Fluid Mechanics 191, 197–223.

Poncet, P., 2004. Topological aspects of three-dimensional wakes behind rotary oscillating cylinders. Journal of Fluid Mechanics 517, 27–53.

Roshko, A., 1954. On the development of turbulent wakes from vortex streets. NACA Report 1191.

Roshko, A., 1993. Perspectives on bluff body aerodynamics. Journal of Wind Engineering and Industrial Aerodynamics 49, 79–100.

Sarpkaya, T., 1986. Force on a circular cylinder in viscous oscillatory flow at low Keulegan-Carpenter numbers. Journal of Fluid Mechanics 165, 61–71.

Sarpkaya, T., 2001. On the force decompositions of Lighthill and Morrison. Journal of Fluids and Structures 15, 227–233.

Schlichting, H., 1951. Grenzschict-Theorie. Reissued as Boundary-Layer Theory, seventh ed., 1987, McGraw-Hill, New York.

Stansby, P.K., Rainey, R.C.T., 2001. On the orbital response of a rotating cylinder in a current. Journal of Fluid Mechanics 439, 87–108.

Teschauer, I., Schäfer, M., Kempf, A., 2002. Numerical simulation of flow induced by a cylinder orbiting in a large vessel. Journal of Fluids and Structures 16, 435–451.

Tokumaru, P.T., Dimotakis, P.E., 1991. Rotary oscillation control of a cylinder wake. Journal of Fluid Mechanics 224, 77–90.

Williamson, C.H.K., Govardhan, R., 2004. Vortex-induced vibrations. Annual Review of Fluid Mechanics 36, 413–455.

Williamson, C.H.K., Roshko, A., 1988. Vortex formation in the wake of an oscillating cylinder. Journal of Fluids and Structures 2, 355–381.

Williamson, C.H.K., Hess, P., Peter, M., Govardhan, R., 1998. Fluid loading and vortex dynamics for a body in elliptic orbits. Paper presented at the Conference on Bluff Body Wakes and Vortex-Induced Vibration, Washington, DC, USA, paper number 18.